

Rap2 and TNIK control Plexin-dependent tiled synaptic innervation in *C. elegans*

Xi Chen¹, Akihiro CE Shibata^{2†}, Ardalan Hendi^{1†}, Mizuki Kurashina¹,
Ethan Fortes¹, Nicholas L Weilinger³, Brian A MacVicar³, Hideji Murakoshi²,
Kota Mizumoto^{1*}

¹Department of Zoology, The University of British Columbia, Vancouver, Canada;
²Supportive Center for Brain Research, National Institute for Physiological Sciences, Okazaki, Japan; ³Department of Psychiatry, The University of British Columbia, Vancouver, Canada

Abstract During development, neurons form synapses with their fate-determined targets. While we begin to elucidate the mechanisms by which extracellular ligand-receptor interactions enhance synapse specificity by inhibiting synaptogenesis, our knowledge about their intracellular mechanisms remains limited. Here we show that Rap2 GTPase (*rap-2*) and its effector, TNIK (*mig-15*), act genetically downstream of Plexin (*plx-1*) to restrict presynaptic assembly and to form tiled synaptic innervation in *C. elegans*. Both constitutively GTP- and GDP-forms of *rap-2* mutants exhibit synaptic tiling defects as *plx-1* mutants, suggesting that cycling of the RAP-2 nucleotide state is critical for synapse inhibition. Consistently, PLX-1 suppresses local RAP-2 activity. Excessive ectopic synapse formation in *mig-15* mutants causes a severe synaptic tiling defect. Conversely, overexpression of *mig-15* strongly inhibited synapse formation, suggesting that *mig-15* is a negative regulator of synapse formation. These results reveal that subcellular regulation of small GTPase activity by Plexin shapes proper synapse patterning in vivo.

DOI: <https://doi.org/10.7554/eLife.38801.001>

***For correspondence:**

mizumoto@zoology.ubc.ca

[†]These authors contributed equally to this work

Competing interests: The authors declare that no competing interests exist.

Funding: See page 20

Received: 31 May 2018

Accepted: 11 July 2018

Published: 31 July 2018

Reviewing editor: Piali Sengupta, Brandeis University, United States

© Copyright Chen et al. This article is distributed under the terms of the [Creative Commons Attribution License](https://creativecommons.org/licenses/by/4.0/), which permits unrestricted use and redistribution provided that the original author and source are credited.

Introduction

During nervous system development, various instructive and repulsive signaling cues cooperatively direct neurons to form chemical synapses with their appropriate targets. Studies have identified some molecules and elucidated their downstream mechanisms that instruct synaptogenesis such as FGF, Ephrin/Eph, Ig-family of cell adhesion molecules (IgCAMs) and synaptic cell adhesion molecules (SynCAMs) (Shen and Bargmann, 2003; Shen et al., 2004; Dabrowski and Umemori, 2016; Dabrowski et al., 2015; Feng et al., 2000; Kayser et al., 2008; Terauchi et al., 2010; Yamagata et al., 2003). Several axon guidance cues and their receptors also play critical roles to inhibit synapse formation (Inaki et al., 2007; Klassen and Shen, 2007; Poon et al., 2008). Semaphorins (Sema) and their receptors, Plexins, are two conserved families of molecules that have a well-established function to repel axons during development (Kolodkin et al., 1993, 1992; Negishi et al., 2005a; Tran et al., 2007) and play prominent roles contributing to immune system, cardiovascular development and cancer regulation (Epstein et al., 2015; Neufeld et al., 2005; Takamatsu and Kumanogoh, 2012).

In addition to its function as a long-range axon guidance cue during neuronal development, Sema/Plexin signaling plays a critical role as a negative regulator of synapse formation. The role of Sema/Plexin signaling to inhibit synapse formation was first observed in *Drosophila*, where ectopic expression of Sema2a causes elimination of specific neuromuscular junctions (Matthes et al., 1995). In mammals, Sema3E/PlexinD1 specifies sensory-motor connections (Pecho-Vrieseling et al., 2009). Secreted Sema3F locally inhibits spine development through its receptors PlexinA3 and Neuropilin-2

eLife digest Genes do more than just direct the color of our hair or eyes. They produce proteins that are involved in almost every process in the body. In humans, the majority of active genes can be found in the brain, where they help it to develop and work properly – effectively controlling how we move and behave.

The brain's functional units, the nerve cells or neurons, communicate with each other by releasing messenger molecules in the gap between them, the synapse. These molecules are then picked up from specific receptor proteins of the receiving neuron.

In the nervous system, neurons only form synapses with the cells they need to connect with, even though they are surrounded by many more cells. This implies that they use specific mechanisms to stop neurons from forming synapses with incorrect target cells. This is important, because if too many synapses were present or if synapses formed with incorrect target cells, it would compromise the information flow in the nervous system. This would ultimately lead to various neurological conditions, including Autism Spectrum Disorder.

In 2013, researchers found that in the roundworm *Caenorhabditis elegans*, a receptor protein called Plexin, is located at the surface of the neurons and can inhibit the formation of nearby synapses. Now, Chen et al. – including one author involved in the previous research – wanted to find out what genes Plexin manipulates when it stops synapses from growing. Knowing what each of those genes does can help us understand how neurons can inhibit synapses.

The results revealed that Plexin appears to regulate two genes, Rap2 and TNIK. Plexin reduced the activity of Rap2 in the neuron that released the messenger, which hindered the formation of synapses. The gene TNIK and its protein on the other hand, have the ability to modify other proteins and could so inhibit the growth of synapses. When TNIK was experimentally removed, the number of synapses increased, but when its activity was increased, the number of synapses was strongly reduced.

These findings could help scientists understand how mutations in Rap2 or TNIK can lead to various neurological conditions. A next step will be to test if these genes also affect the formation of synapses in other species such as mice, which have a more complex nervous system that is structurally and functionally more similar to that of humans.

DOI: <https://doi.org/10.7554/eLife.38801.002>

in hippocampal granule cells (*Tran et al., 2009*). Sema5A/PlexinA2 signaling inhibits excitatory synapse formation in dentate granule cells (*Duan et al., 2014*). Sema5B diminishes synaptic connections in cultured hippocampal neurons (*O'Connor et al., 2009*). However, little is known about the intracellular mechanisms through which Sema/Plexin signaling inhibits synapse formation.

The cytoplasmic domain of Plexin contains a GAP (GTPase-activating protein) domain that inactivates small GTPases (*Oinuma et al., 2004; Rohm et al., 2000*). Upon activation by Semaphorins, Plexins repel axon outgrowth by inhibiting R-Ras (*Negishi et al., 2005b; Hota and Buck, 2012; Tasaka et al., 2012*). Recent biochemical and structural analyses demonstrated that the GAP domain of mammalian PlexinA3 is specific for Rap GTPases, which belong to the Ras family of GTPases and regulate the actin cytoskeleton (*Wang et al., 2012, 2013*). PlexinA3 dimerization by Semaphorin activates its GAP domain, thereby inhibiting Rap1 from inducing neurite retraction. Drosophila PlexA and zebrafish PlexinA1 promote remodeling of epithelial cells by inhibiting Rap1 GTPase during wound healing (*Yoo et al., 2016*). Another Rap GTPase, Rap2, can inhibit neurite outgrowth (*Kawabe et al., 2010*). Similar to Sema/Plexin signaling, Rap GTPases regulate synapse formation and function. Rap2 negatively regulate spine number in cultured hippocampal neurons (*Fu et al., 2007*). Rap1 and Rap2 regulate synaptic activity by removing AMPA receptors from spines during long-term depression and depotentiation, respectively (*Zhu et al., 2002, Zhu et al., 2005*). While the GAP domain of Plexin is critical to inhibit synapse formation (*Duan et al., 2014; Mizumoto and Shen, 2013a*), we still do not know whether Plexin regulates synapse patterning via Rap GTPases at presynaptic sites.

In *Caenorhabditis elegans*, Sema/Plexin signaling functions in vulva formation and male ray development (*Dalpé et al., 2005, 2004; Fujii et al., 2002; Ikegami et al., 2004; Liu et al., 2005;*

Nakao et al., 2007; Nukazuka et al., 2008, 2011). Using this model system, we previously reported that Sema/Plexin signaling in the nervous system mediates a critical inter-axonal interaction for the tiled synaptic innervation of two DA-class cholinergic motor neurons (DA8 and DA9) (*Mizumoto and Shen, 2013a*). Cell bodies of nine DA neurons in *C. elegans* reside in the ventral nerve cord, sending dendrites ventrally and axons dorsally to form *en passant* synapses onto the dorsal body wall muscles. Even though axons of DA neurons show significant overlap, each motor neuron forms synapses onto muscles within specific sub-axonal domains, which do not overlap with those from neighboring DA neurons. This unique synaptic innervation creates tiled synaptic patterns along the nerve cord (*White et al., 1986*).

Tiled synaptic innervation occurs within most motor neuron classes and may contribute to the sinusoidal locomotion pattern of *C. elegans* (*White et al., 1986*). Using a combination of two fluorescent proteins (GFP and mCherry) fused with the presynaptic vesicle protein, RAB-3, and two tissue specific promoters (*Figure 1*) (*Mizumoto and Shen, 2013a*), we can visualize this synaptic tiling between DA8 and DA9 neurons. We reported that PLX-1 localizes at the anterior edge of the DA9 synaptic domain in axon-axon interactions in a Semaphorin-dependent manner, where it locally inhibits formation of the presynaptic specialization via its GAP domain. Loss of *Semas* or *plx-1* causes anterior expansion of DA9 synaptic domain and posterior expansion of DA8 synaptic domain. This result indicates loss of inter-axonal interactions between DA8 and DA9 neurons. Consistently, Tran et al., also observed excess dendritic spine formation, specifically within the region close to the cell body, in the *plexin* knockout mouse (*Tran et al., 2009*). These findings suggest a conserved mechanism by which Sema/Plexin locally inhibits synapse formation.

We previously reported that *let-60/KRas* gain-of-function mutants showed very mild synaptic tiling defects. Since mammalian Plexin acts as a RapGAP, we hypothesized that Rap GTPase is the major downstream effector of PLX-1 to regulate synaptic tiling of DA neurons. Here, we report that *rap-2*, a *C. elegans* ortholog of human Rap2A, and its effector kinase *mig-15* (TNIK: Traf2- and Nck-interacting kinase) act genetically downstream of *plx-1* to regulate synaptic tiling. PLX-1 delineates the border of synaptic tiling by locally inhibiting RAP-2 along the DA9 axon. We also discovered an unexpected role for *mig-15* in inhibiting synapse formation. Our results reveal the mechanism underlying Plexin signaling to form fine synaptic map connectivity.

Results

***rap-2* functions downstream of *plx-1* to regulate synaptic tiling**

Three Rap genes exist in the *C. elegans* genome (*rap-1*, *rap-2* and *rap-3*). To delineate which Rap GTPase functions downstream of PLX-1 in synaptic tiling between DA8 and DA9 neurons, we first examined the expression patterns of all three *rap* genes (*Figure 1—figure supplement 1*). Among them, only *rap-2*, an ortholog of mammalian Rap2a, was expressed in motor neurons including DA8 and DA9, while *rap-1* and *rap-3* were not expressed in these cells (*Figure 1—figure supplement 1*). In wild type animals, synaptic domains of DA8 and DA9 neurons did not show significant overlap, creating tiled synaptic innervation (*Figure 1A and G*). In the *plx-1(nc36)* null mutant, synaptic domains of DA8 and DA9 expanded posteriorly and anteriorly, respectively. As a result, synaptic domains of these neurons overlapped significantly (*Figure 1B and G*).

Since the intracellular domain of Plexin contains a RapGAP domain, we hypothesized that RAP-2 preferentially exists in a GTP-bound form in the *plx-1* mutants. The G12V mutant is widely used as a constitutively GTP-form of small GTPases including mammalian Rap2A and *C. elegans* RAP-1 (*Kawabe et al., 2010; Pellis-van Berkel et al., 2005*). Expression of a constitutively GTP-bound form of *rap-2(G12V)* under the A-type neuron specific promoter, *Punc-4*, elicited a similar synaptic tiling defect as *plx-1* mutants (*Figure 1C and G*). Expression of wild type *rap-2* under the *unc-4* promoter did not affect the synaptic tiling pattern, suggesting that G12V mutation but not over-expression of *rap-2* caused the synaptic tiling defect (*Figure 1G*). We then generated *rap-2(G12V)* mutants using CRISPR/Cas9 genome editing. We observed the same synaptic tiling defects in three independent *rap-2(G12V)* mutant alleles (*miz16*, *miz17* and *miz18*) as in *plx-1* mutants (*Figure 1D and G* and *Figure 1—figure supplement 2*). We found a comparable level of gene expression among all three *rap-2(G12V)* mutants to wild type *rap-2* using RT-qPCR (*Figure 1—figure supplement 2*). These

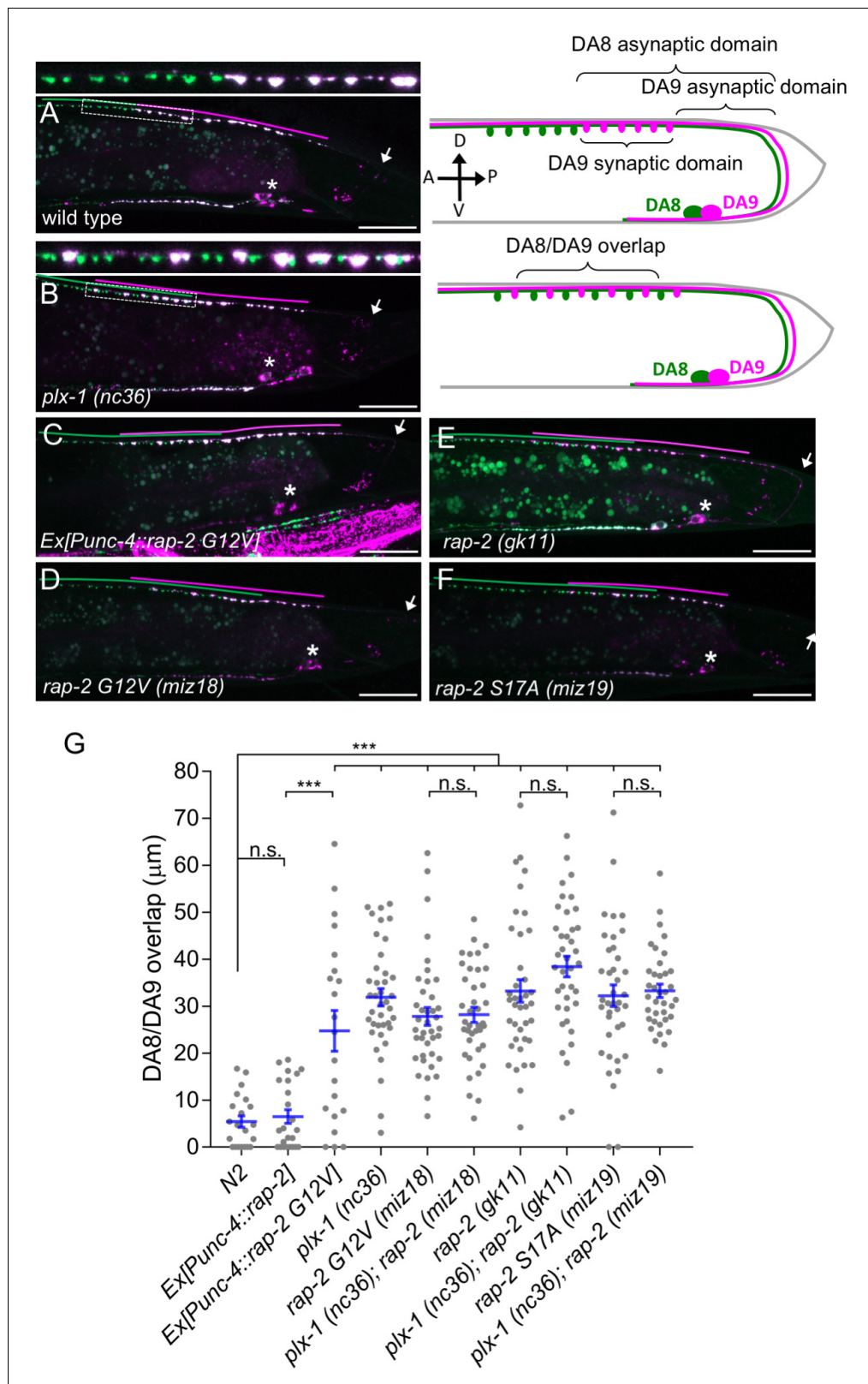


Figure 1. Gain- and loss-of-function *rap-2* mutants show synaptic tiling defects. (A and B) Representative image of synaptic tiling of wild type (A) and *plx-1* mutant (B) animals. Images show *wyls446* marker to label synapses in DA8 (GFP::RAB-3) and DA9 (GFP::RAB-3+mCherry::RAB-3). Dotted box represents the magnified images from A and B of the synaptic tiling border. Schematics of DA8 (green) and DA9 (magenta) neurons with parameters for analysis

Figure 1 continued on next page

Figure 1 continued

shown on the right. (C–F) Representative images of *wyls446* strains with the following genotypes: *rap-2(G12V)* overexpression in DA neurons (C), *rap-2 G12V (miz18)* (D), *rap-2 null (gk11)* (E) and *rap-2 S17A (miz19)* (F). Synaptic domains from DA8 and DA9 are highlighted with green and magenta lines, respectively. Asterisks: DA9 cell body. Arrows: dorsal commissure of DA9. Scale bars: 20 μ m. (G) Quantification of overlap between DA8 and DA9 synaptic domains. Each dot represents a single animal. Blue bars indicate mean \pm SEM. n.s.: not significant; *** $p < 0.001$.

DOI: <https://doi.org/10.7554/eLife.38801.003>

The following figure supplements are available for figure 1:

Figure supplement 1. *rap-1* and *rap-3* are not involved in synaptic tiling of DA8 and DA9.

DOI: <https://doi.org/10.7554/eLife.38801.004>

Figure supplement 2. Synaptic tiling requires both GTP- and GDP-bound forms of RAP-2.

DOI: <https://doi.org/10.7554/eLife.38801.005>

Figure supplement 3. Co-localization between RAB-3 and the active zone markers, CLA-1 and UNC-10.

DOI: <https://doi.org/10.7554/eLife.38801.006>

results confirm that the *rap-2(G12V)* mutation itself, not changes in gene expression, underlie the synaptic tiling defect in *rap-2(G12V)* mutants.

Surprisingly, the null mutant of *rap-2(gk11)* also showed the same synaptic tiling defect, as did the constitutively GTP-form of *rap-2(G12V)* mutants (**Figure 1E and G**). This result suggests that synaptic tiling requires both the GTP- and GDP-bound forms of RAP-2. Indeed, the constitutively GDP-bound form of *rap-2* mutants (S17A: *miz19*, *miz20*) showed the identical synaptic tiling defect as *rap-2(G12V)* and *rap-2(gk11)* mutants (**Figure 1F and G** and **Figure 1—figure supplement 2**). These results suggest that the cycling between GTP- and GDP-forms of RAP-2 is critical to regulate the spatial patterning of synapses.

Similar to *plx-1* mutants, the synaptic tiling defect in all *rap-2* mutants is caused by both the posterior expansion of DA8 synaptic domain and the anterior expansion of the DA9 synaptic domain (**Figure 1—figure supplement 2**). However, none of *rap-2(G12V)*, *rap-2(S17A)* and *rap-2(gk11)* mutants enhanced or suppressed the synaptic tiling defect in *plx-1* mutants (**Figure 1G**). These results suggest that *plx-1* and *rap-2* function in the same genetic pathway. Consistent with the expression patterns of *rap-1* and *rap-3*, neither *rap-1(pk2082)* nor *rap-3(gk3975)* null mutants showed significant synaptic tiling defects by themselves and did not enhance the synaptic tiling defect in *rap-2(gk11)* null mutants (**Figure 1—figure supplement 1**). All mCherry::RAB-3 puncta co-localized with active zone markers, CLA-1 (*Xuan et al., 2017*) and UNC-10/Rim (*Wu et al., 2013*) in the DA9 neurons of *plx-1(nc36)* and *rap-2(gk11)* mutants, suggesting that RAB-3 puncta represent *bona fide* synapses (**Figure 1—figure supplement 3**). Taken together, these data indicate that *plx-1* and *rap-2* act in the same genetic pathway for synaptic tiling in DA neurons.

RAP-2 functions cell autonomously in DA neurons

We next determined the cellular location for *rap-2* function. Since *rap-2(gk11)* null mutants showed a synaptic tiling defect, we conducted tissue specific rescue experiments using tissue-specific promoters as previously described (*Mizumoto and Shen, 2013a*). Expression of *rap-2* in the post-synaptic body wall muscle cells under the *hlh-1* promoter or in another class of cholinergic motor neurons in the dorsal nerve cord (DB neurons) under the truncated *unc-129* promoter did not rescue the synaptic tiling defect in *rap-2(gk11)* animals (**Figure 2A, B and G**). However, DA neuron-specific expression using the *unc-4c* promoter strongly rescued the synaptic tiling defect (**Figure 2C and G**). DA9-specific expression of *rap-2* under the *mig-13* promoter partially rescued the synaptic tiling defect (**Figure 2E and G**). DA9-specific expression of *rap-2* rescued the phenotype of anterior expansion of the DA9 synaptic domain but not the posterior expansion of DA8 synaptic domain (**Figure 2H and I**). These results suggest that *rap-2* regulates synapse patterning in a cell-autonomous manner. In contrast to the DA9-specific rescue experiment in *rap-2* mutants, DA9-specific expression of *plx-1* cDNA was sufficient to rescue synaptic defects in both DA9 and DA8 (*Mizumoto and Shen, 2013a*) (see Discussion).

We also observed that expression of human Rap2a in DA neurons rescued the synaptic tiling defect of *rap-2* mutants, suggesting the function of *rap-2* in synapse patterning is conserved across

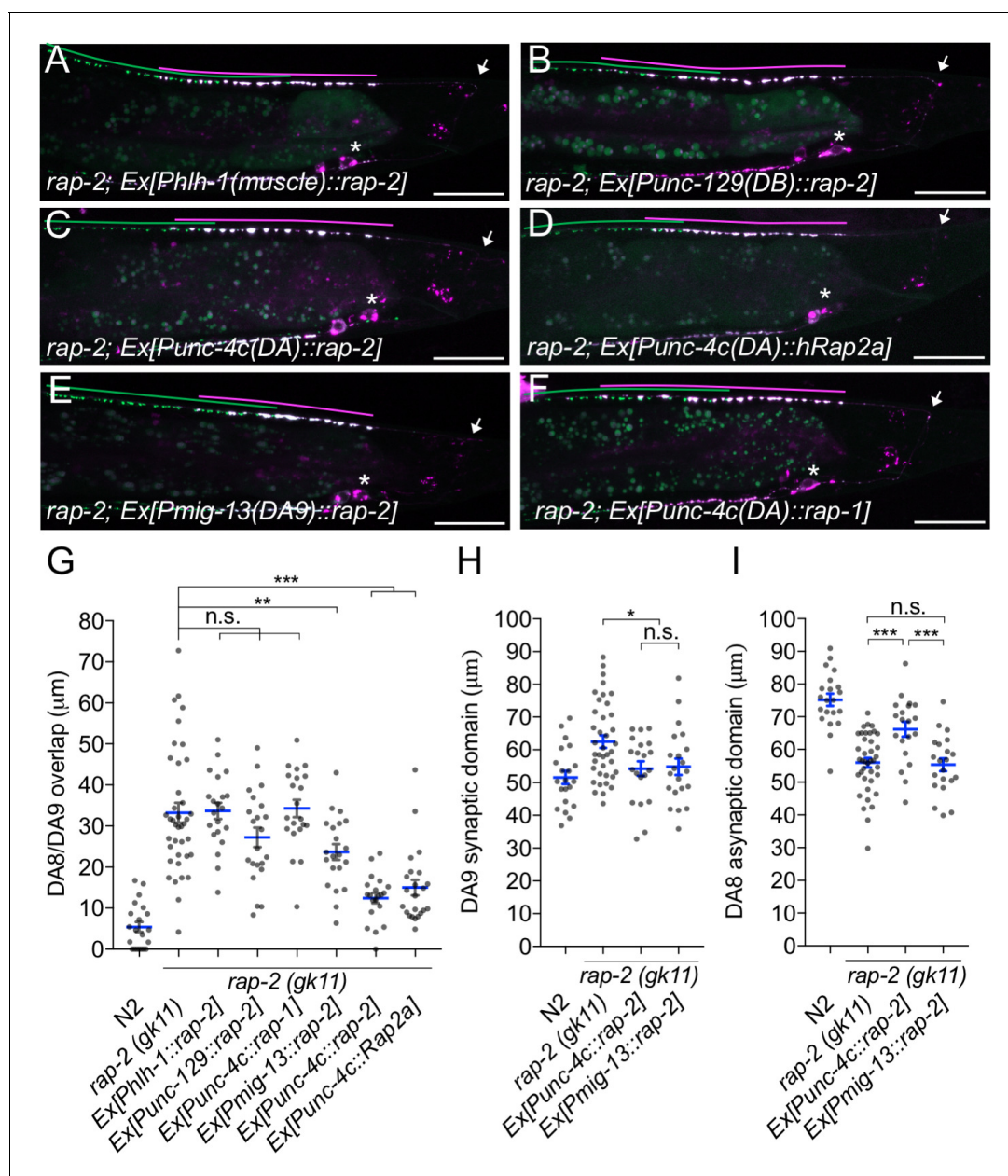


Figure 2. *rap-2* functions in DA neurons. (A–F) Representative images of *rap-2*; *wyls446* animals expressing *Phlh-1::rap-2* (A), *Punc-129::rap-2* (B), *Punc-4c::rap-2* (C), *Punc-4c::Rap2a* (human) (D), *Pmig-13::rap-2* (E) and *Punc-4c::rap-1* (F). Synaptic domains of DA8 and DA9 are highlighted with green and magenta lines, respectively. Asterisks: DA9 cell body. Arrows: dorsal commissure of DA9. Scale bars: 20 μm. (G–I) Quantification of DA8/DA9 overlap (G), DA9 synaptic domain (H) and DA8 asynaptic domain (I). Each dot represents a single animal. Blue bars indicate mean ± SEM. n.s.: not significant; ***p < 0.001; **p < 0.01; *p < 0.05.

DOI: <https://doi.org/10.7554/eLife.38801.007>

species (Figure 2D and G). Previous work suggested a partial functional redundancy between *rap-1* and *rap-2* in *C. elegans* (Pellis-van Berkel et al., 2005). However, we found that *rap-1* expression in DA neurons did not rescue the synaptic tiling defect of *rap-2* mutants, suggesting functional diversity between *rap-1* and *rap-2* (Figure 2F and G). Taken together, we conclude that *rap-2* functions cell autonomously in DA neurons to regulate synaptic tiling.

RAP-2 activity is spatially regulated by PLX-1

Previously, we demonstrated that PLX-1::GFP is localized at the anterior edge of the DA9 synaptic domain, where it negatively regulates synapse formation through its cytoplasmic GAP domain (**Figure 3A and E**) (**Mizumoto and Shen, 2013a**). In the *rap-2(gk11)* mutant background, we observed no change in PLX-1::GFP localization but did observe ectopic synapses in the axonal region anterior to the PLX-1::GFP domain (**Figure 3B and F**). This result is consistent with our hypothesis that *rap-2* acts downstream of *plx-1* to regulate synaptic tiling. Together with our finding that synaptic tiling requires both GTP- and GDP-bound forms of RAP-2, we speculate that PLX-1 acting at the anterior edge of the DA9 synaptic domain regulates the spatial activity of RAP-2 along the axon.

We then sought to determine the spatial distribution of GTP-RAP-2 in DA9 axon. We conducted Fluorescence Lifetime Imaging Microscopy (FLIM)-based FRET (Förster Resonance Energy Transfer) measurements using EGFP-Rap2A (human) and mRFP-RalGDS(RBD: Ras Binding Domain)-mRFP (**Yasuda et al., 2006**). As RalGDS-RBD specifically binds to GTP-Rap2 but not GDP-Rap2 (**Ohba et al., 2000**), FRET from EGFP-Rap2A to mRFP-RalGDS(RBD)-mRFP can be used as a readout of Rap2 activity. We detected FRET signal as a change of GFP fluorescence lifetime (**Figure 4A**). In HeLa cells, we observed a shorter lifetime of constitutively bound GTP construct EGFP-Rap2A(G12V) compared to GDP-bound EGFP-Rap2A(S17A), indicating that the FRET sensor can detect the nucleotide state of Rap2A (**Figure 4B and C**). Due to the low expression of *C. elegans* RAP-2 constructs in HeLa cells, we were not able to test whether the mammalian FRET sensor can detect *C. elegans* RAP-2 activity (data not shown).

We then expressed EGFP-Rap2A and mRFP-RalGDS(RBD)-mRFP FRET sensors in DA9 neurons in *C. elegans*. As human Rap2a rescued the synaptic tiling defect of *rap-2(gk11)* mutants (**Figure 2G**), we reasoned that the activity pattern of human Rap2A should recapitulate that of endogenous RAP-2. We indeed observed lower Rap2A activity at the anterior edge of the DA9 synaptic domain compared to within the synaptic domain (**Figure 4D and F**). This observation is consistent with the localization of PLX-1::GFP at the anterior edge of DA9 synaptic domain (**Figure 3A**) (**Mizumoto and Shen, 2013a**). Local inhibition of Rap2a activity was strongly diminished in the *plx-1* mutant background (**Figure 4D and F**). Higher Rap2 activity in the synaptic region could simply indicate the presence of synapses within the synaptic domain, rather than Rap2 inactivation by Plexin at the anterior edge of the synaptic domain. To exclude this possibility, we examined Rap2 activity in *unc-104/Kif1A* mutants, which show no synapses are formed in DA9 axon (**Ou et al., 2010**). We showed previously that PLX-1::GFP localization to the synaptic tiling border was independent of synapses, since it was unaffected in *unc-104/Kif1A* mutants (**Mizumoto and Shen, 2013a**). In *unc-104* mutants, we observed the same local inhibition of Rap2A activity at the putative synaptic tiling border, but not in *unc-104; plx-1* double mutants (**Figure 4E and G**), indicating that Plexin controls local Rap2 activity independent of synapses.

To understand that this local Rap2 inactivation at the synaptic tiling border depends on the localized RapGAP activity of PLX-1, we examined the rescue activity of two PLX-1 mutant constructs, PLX-1(RA) and PLX-1(Δ Sema), neither of which rescued the synaptic tiling defect of *plx-1* mutants (**Mizumoto and Shen, 2013a**). PLX-1(RA) is a GAP-deficient mutant but localizes normally at the anterior edge of the DA9 synaptic domain. PLX-1(Δ Sema) contains intact GAP domain but cannot be activated by the endogenous ligand and shows diffused localization due to deletion of the extracellular SEMA domain (**Mizumoto and Shen, 2013a**). We observed no local Rap2 inactivation in *plx-1* mutant animals expressing these mutant PLX-1 constructs in DA9, while expression of wild type PLX-1 cDNA rescued local Rap2 inactivation at the anterior edge of the DA9 synaptic domain (**Figure 4H**).

While we do not fully exclude the possibility that PLX-1 indirectly regulates local Rap2 activity, these data taken together with the biochemical evidence that mammalian Plexin acts as RapGAP (**Wang et al., 2013, 2012**) strongly suggests that Plexin localized at the anterior edge of the DA9 synaptic domain locally inactivates Rap2 GTPase to delineate the synaptic tiling border in DA9.

mig-15(TNIK) regulates synaptic tiling

In mammals, TNIK (Traf2 and Nck1-interacting kinase) acts with Rap2 to regulate neurite extension, AMPA receptor trafficking in hippocampal neurons and microvilli formation in intestinal cells

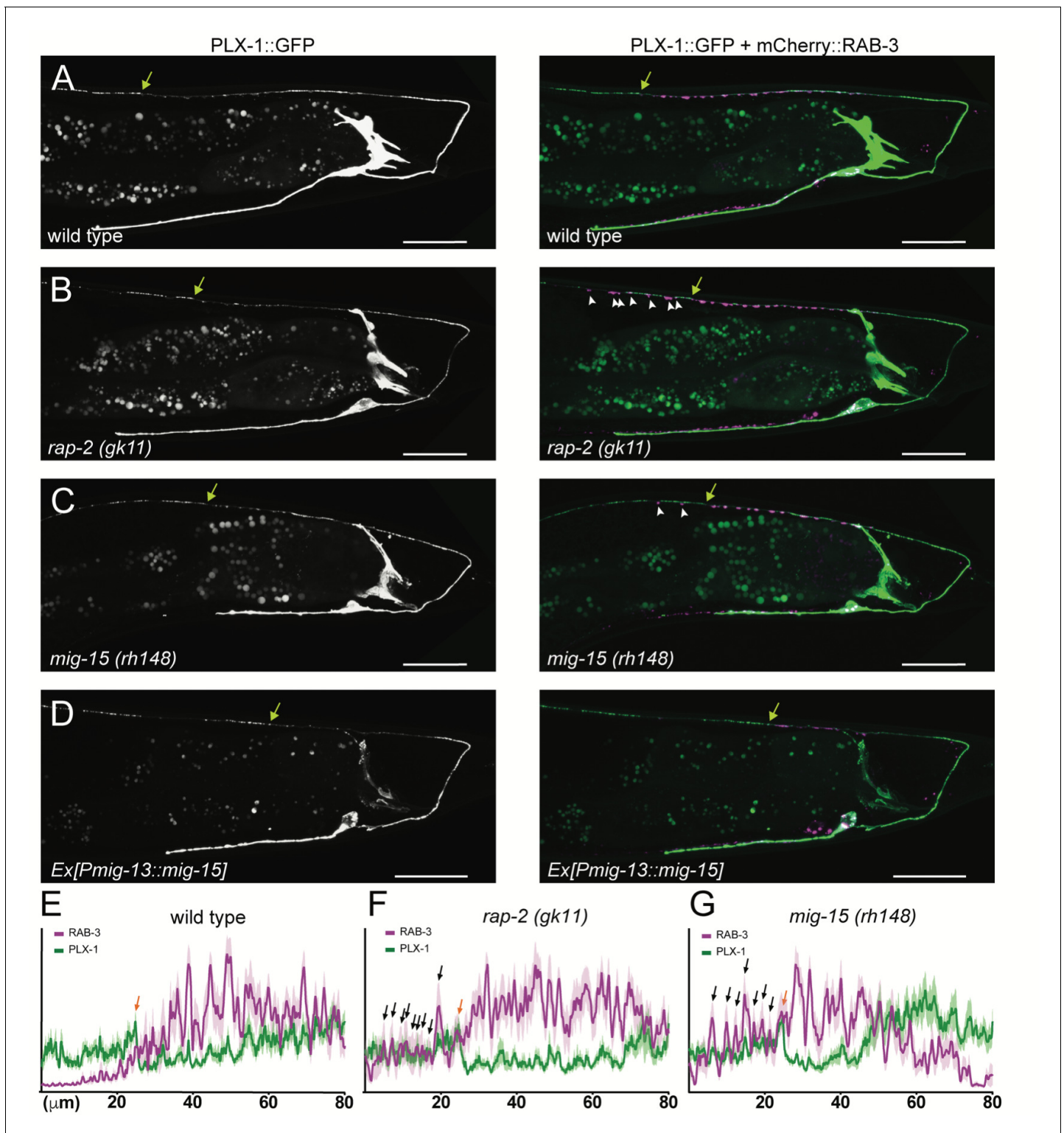


Figure 3. PLX-1::GFP localization is not affected in *rap-2* and *mig-15* mutants. (A–D) Representative image of PLX-1::GFP alone (top) and PLX-1::GFP with mCherry::RAB-3 (middle) labeled with *wyls320* in DA9 of wildtype (A), *rap-2(gk11)* (B) and *mig-15(rh148)* (C). Bracket indicates the PLX-1::GFP patch localized at the anterior edge of the DA9 synaptic domain. Arrowheads indicate ectopic synapses formed anterior to the PLX-1::GFP patch. Scale bars: 20 μm. (E–G) Quantification of the normalized mCherry::RAB-3 signal (magenta) and PLX-1::GFP signal (green) in the dorsal axon of DA9 in wildtype (E), *rap-2(gk11)* (F) and *mig-15(rh148)* (G). Animals were aligned according to the PLX-1::GFP patch at the anterior edge of the DA9 synaptic domain (orange arrow). Light colors indicate SEM.

DOI: <https://doi.org/10.7554/eLife.38801.008>

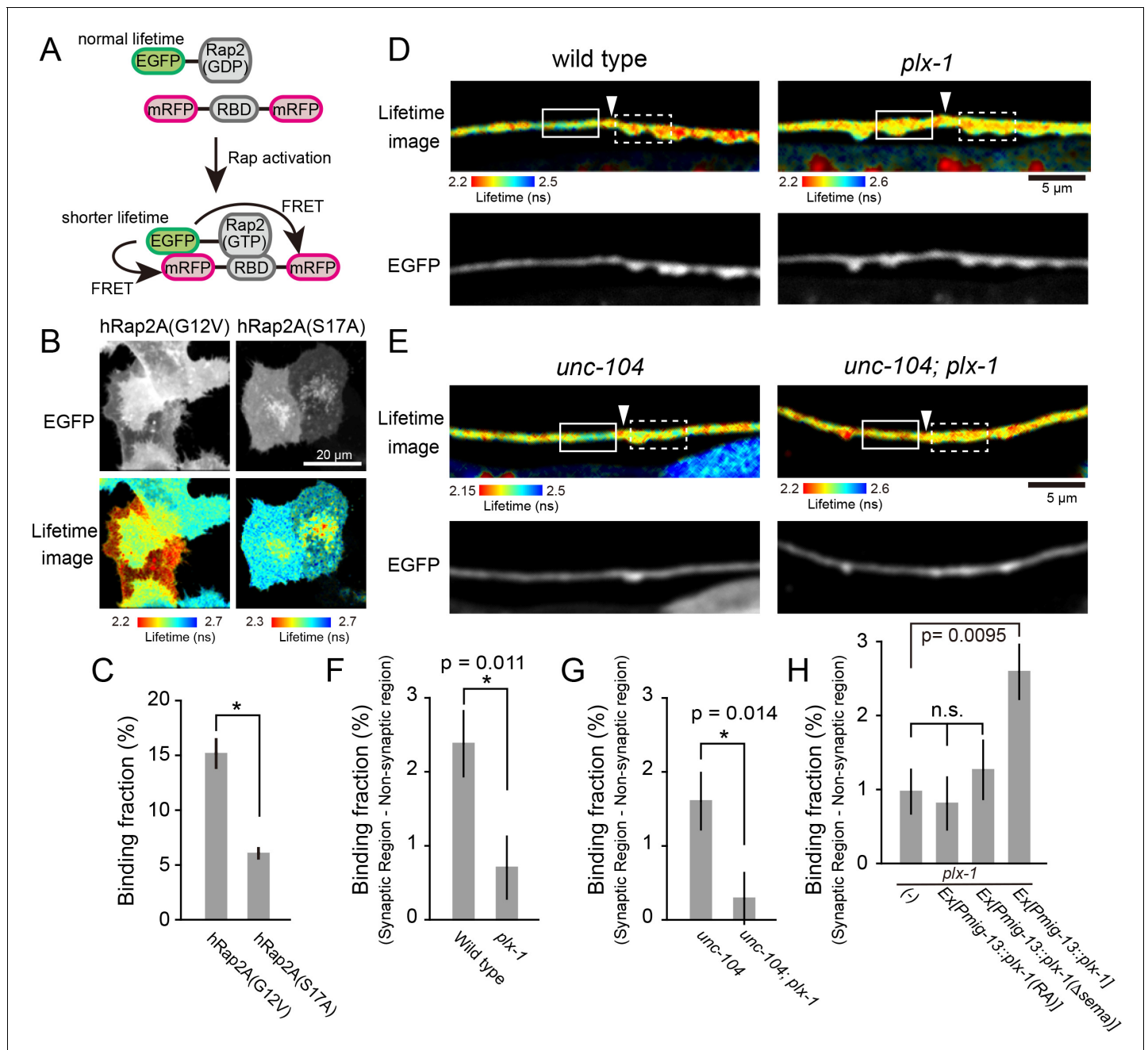


Figure 4. PLX-1 locally inhibits Rap2 activity in DA9. (A) Schematic of Rap2 FRET sensor system. Binding of mRFP- RalGDS(RBD)-mRFP to EGFP-Rap2 induces FRET from EGFP to mRFP, leading to decreased EGFP fluorescence lifetime. (B) Representative fluorescence (top) and fluorescence lifetime images (bottom) of HeLa cells expressing Rap2 FRET sensor (mRFP-RalGDS(RBD)-mRFP) with either constitutively GTP(G12V)- or GDP(S17A)- forms of human Rap2A. (C) Quantification of the binding fraction of Rap2 mutants in HeLa cells. Binding fractions measured from fluorescence decay curves of individual cells (G12V, n = 25; S17A, n = 25), as described previously (Murakoshi et al., 2011). Data shown as mean \pm SEM. Asterisks denote statistical significance ($p < 0.05$, student's t-test). (D) Representative images of fluorescence lifetime (top) and fluorescence (bottom) of *miz1s19* in wild type (left) and *plx-1* mutants (right). White arrowheads indicate the position of the putative synaptic tiling border, as judged by the slight dorsal shift of the DA9 axon, as reported previously (Mizumoto and Shen, 2013a). (E) Representative images of fluorescence lifetime (top) and fluorescence (bottom) of *miz1s19* in *unc-104* (left) and *unc-104; plx-1* double mutants (right). (F) Quantification of the difference in binding fraction of GTP-Rap2a and RalGDS (RBD) between synaptic region (dotted boxes in D) and anterior asynaptic region (solid boxes in D). The binding fraction measured in synaptic region (dotted rectangle) was subtracted by that in non-synaptic region (solid rectangle). Five micrometers along the axon line from the synaptic tiling border were used for quantification. Data presented as mean \pm SEM (wild type, n = 22; *plx-1*, n = 17). (G) Quantification of the difference in binding fraction of GTP-Rap2A and RalGDS(RBD) between synaptic region (dotted boxes in E) and anterior asynaptic region (solid boxes in E). The binding fraction measured in synaptic region (dotted rectangle) subtracted from that in non-synaptic region (solid rectangle). Five micrometers along the axon line from

Figure 4 continued on next page

Figure 4 continued

the synaptic tiling border were used for quantification. Data are presented as mean \pm SEM (*unc-104*, $n = 21$; *unc-104; plx-1*, $n = 23$). (H) Quantification of the difference in binding fraction of GTP-Rap2a and RalGDS(RBD) between synaptic region and anterior asynaptic region in *plx-1* mutants and *plx-1* mutants expressing rescuing constructs. Five micrometers along the axon line from the synaptic tiling border were used for quantification. Data are presented as mean \pm SEM (*no array*, $n = 35$; *Ex[Pmig-13::plx-1(RA)]*, $n = 39$; *Ex[Pmig-13::plx-1(Δ sema)]*, $n = 41$; *Ex[Pmig-13::plx-1]*, $n = 51$).

DOI: <https://doi.org/10.7554/eLife.38801.009>

(Hussain et al., 2010; Kawabe et al., 2010; Gloerich et al., 2012). In *C. elegans*, *mig-15* is the sole ortholog of mammalian TNIK and its paralog MINK1 (Misshapen-like kinase 1), which also is an effector of Rap GTPase (Nonaka et al., 2008). *mig-15* can regulate various cellular processes, such as axon guidance and cell migration (Chapman et al., 2008; Poinat et al., 2002; Shakir et al., 2006; Teulière et al., 2011). We found that *mig-15(rh148)* hypomorphic mutants showed a severe synaptic tiling defect (Figure 5A and D). Similar to *plx-1* and *rap-2* mutants, the synaptic tiling defect followed the anterior expansion of the DA9 synaptic domain and the posterior expansion of the DA8 synaptic domain (Figure 5E and F). All RAB-3 puncta in *mig-15(rh148)* mutants co-localized with active zone markers, CLA-1 and UNC-10 (Figure 1—figure supplement 3), suggesting that these RAB-3 puncta represent bona fide synapses. We observed axon guidance defects (23%, $n = 100$) or ectopic branch formation (56%, $n = 100$) in DA9 of *mig-15* mutant animals (Figure 5—figure supplement 1). These were excluded from our analysis of synaptic tiling phenotypes. While only half of the *mig-15* mutant animals showed axon guidance defects or ectopic branch formation, the synaptic tiling defect of *mig-15* mutants was almost fully penetrant (Figure 5D). We did not observe significant synaptic tiling defects in *cdh-4(rh310)* mutants (DA8/DA9 overlap: $4.6 \pm 1.02 \mu\text{m}$, $n = 21$), which can exhibit an axon defasciculation phenotype in the dorsal nerve cord neurons (Schmitz et al., 2008). These data suggest that the synaptic tiling defect in the *mig-15* mutants is not a secondary effect of axon outgrowth and guidance.

The other two nonsense alleles (*rh326: Q439Stop*, *rh80: W898Stop*) also showed identical synaptic tiling defects as *mig-15(rh148)* (Figure 5—figure supplement 2). *mig-15(rh80)* has a nonsense mutation within the highly conserved CNH (citron/NIK homology) domain, which is required to interact with Rap2 in both mammals and *C. elegans* (Taira et al., 2004). This suggests a physical interaction between RAP-2 and MIG-15 for synaptic tiling. *plx-1* or *rap-2* mutants did not enhance the synaptic tiling defect in *mig-15* mutants (Figure 5B–F). This result is consistent with our hypothesis that *mig-15* acts in the same genetic pathway as *plx-1* and *rap-2*. The PLX-1::GFP patch at the putative synaptic tiling border was unaffected in *mig-15* mutants, even though the position of the PLX-1::GFP patch has shifted slightly posteriorly compared with wild type (Figure 3C and G). Taken together, these results suggest that *mig-15* acts downstream of *plx-1* to regulate synaptic tiling.

Interestingly, the degree of overlap between DA8 and DA9 synaptic domains was even larger in *mig-15* mutants than those observed in *plx-1* and *rap-2* mutants (compare Figures 1G and 5D), suggesting that *mig-15* also acts downstream of additional signaling pathways (see discussion).

***mig-15* functions in DA neurons**

We then determined in which cells *mig-15* functions by conducting tissue specific rescue experiments. Since several *mig-15* isoforms (wormbase and data not shown) exist, we used the *mig-15* genomic sequence for the rescue experiments. Expression of *mig-15* under the DA neuron specific promoter (*Punc-4c*) strongly rescued the synaptic tiling defect of *mig-15(rh148)* mutants (Figure 6A and F), consistent with our hypothesis that *mig-15* acts in the same genetic pathway as *plx-1* and *rap-2*.

Expression of *mig-15* in both DA8 and DA9 rescued both posterior expansion of the DA8 synaptic domain and anterior expansion of the DA9 synaptic domain (Figure 6G and H). DA9 specific expression of *mig-15* under the *mig-13* promoter rescued anterior expansion of the DA9 synaptic domain, suggesting that *mig-15* functions cell autonomously in DA9 (Figure 6B and G). We observed that *Pmig-13::mig-15* weakly rescued the posterior expansion of the DA8 synaptic domain (Figure 6H). This is likely due to the leaky expression of *mig-15* in DA8, as the *mig-15* genomic fragment without promoter showed slight rescue of the synaptic tiling defect in *mig-15(rh148)* mutants (Figure 6F). Kinase dead TNIK mutants act as a dominant-negative (Mahmoudi et al., 2009). In DA

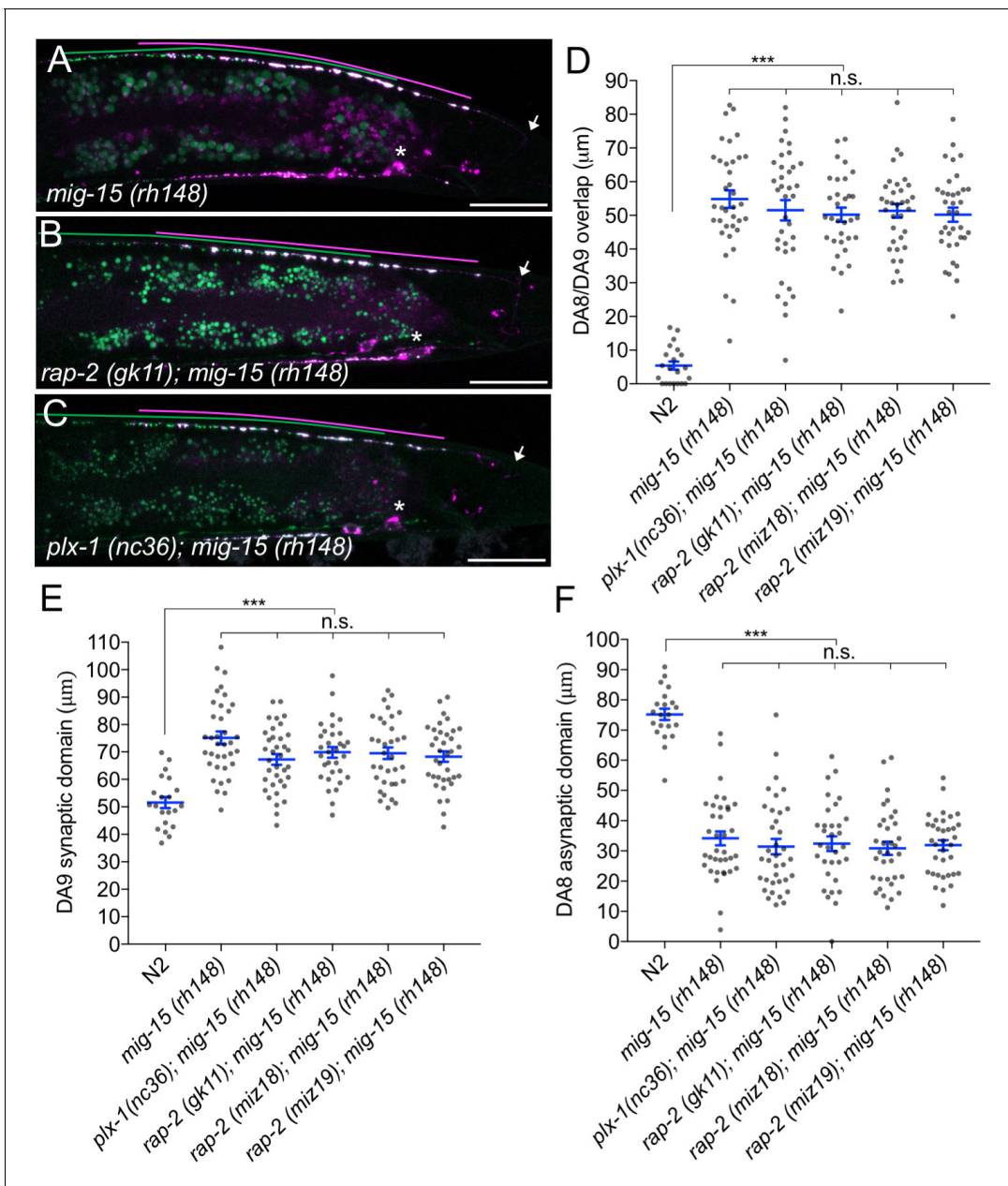


Figure 5. *mig-5(TNIK)* mutants show a severe synaptic tiling defect. (A–C) Representative images of synaptic tiling marker (*wyls446*) in *mig-5(rh148)* (A), *rap-2(gk11); mig-5(rh148)* (B) and *plx-1(nc36); mig-5(rh148)* (C) mutants. Synaptic domains of DA8 and DA9 are highlighted with green and magenta lines, respectively. Asterisks: DA9 cell body. Arrows: dorsal commissure of DA9. Scale bars: 20 μm. (D–F) Quantification of overlap between DA8 and DA9 synaptic domains (D), DA9 synaptic domain (E) and DA8 asynaptic domain (F) in respective mutant backgrounds. Each dot represents measurement from a single animal. Blue bars indicate mean ± SEM. n.s.: not significant; ****p*<0.001.

DOI: <https://doi.org/10.7554/eLife.38801.010>

The following figure supplements are available for figure 5:

Figure supplement 1. Morphological defects of DA9 axon in *mig-5(rh148)* mutants.

DOI: <https://doi.org/10.7554/eLife.38801.011>

Figure supplement 2. Synaptic tiling defect in *mig-5* mutants.

DOI: <https://doi.org/10.7554/eLife.38801.012>

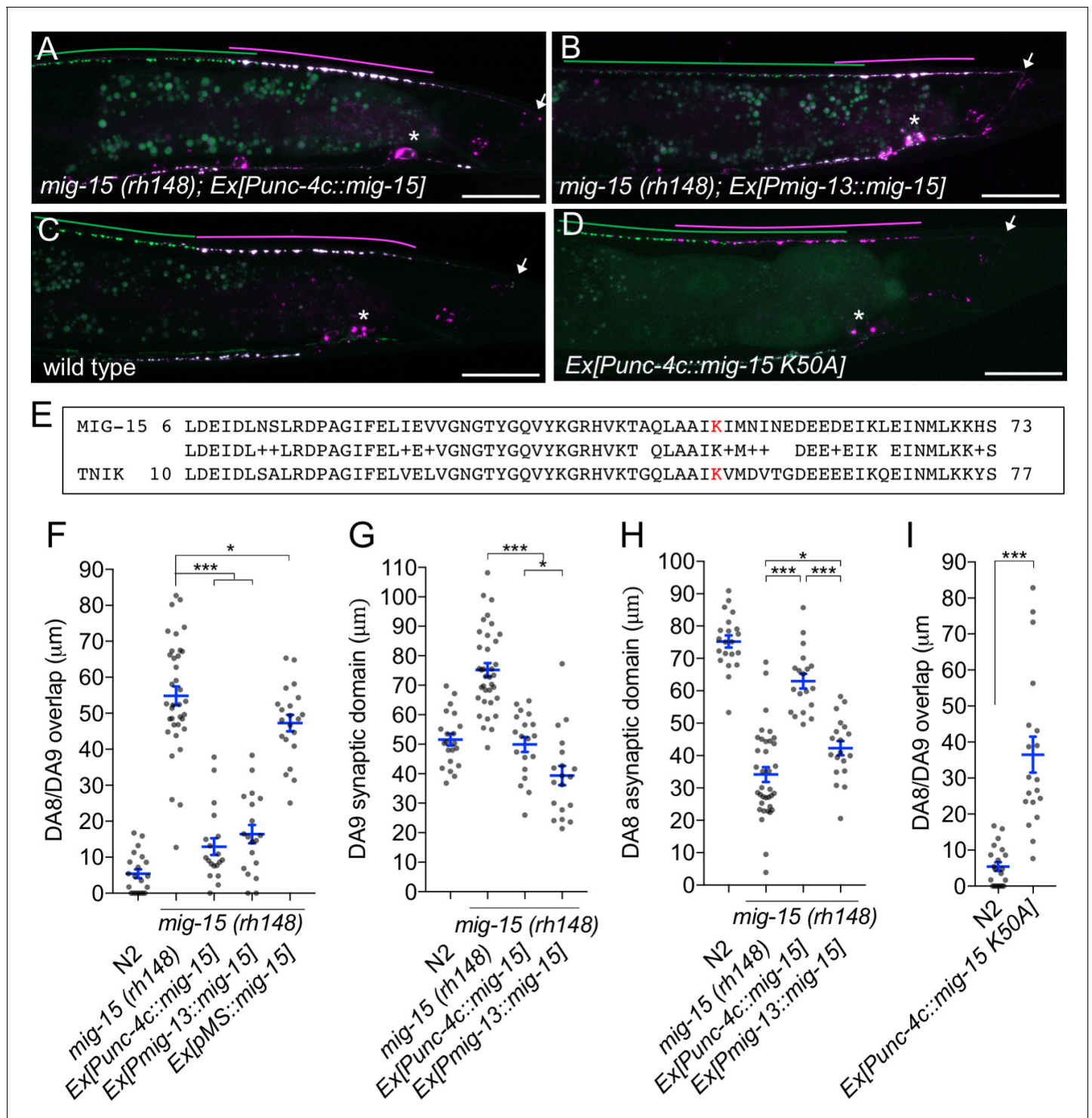


Figure 6. *mig-15* functions in DA neurons. (A–D) Representative images of synaptic tiling marker (*wyls446*) in the following backgrounds: *mig-15(rh148); Ex[Punc-4c::mig-15]* (A), *mig-15(rh148); Ex[Pmig-13::mig-15]* (B), wild type (C) and wild type animals expressing dominant-negative *mig-15(K50A)* in DA neurons (D). Synaptic domains of DA8 and DA9 are highlighted with green and magenta lines, respectively. Asterisks: DA9 cell body. Arrows: dorsal commissure of DA9. Scale bars: 20 μm. (E) Amino acid alignment of amino-terminal region of MIG-15 and TNIK. A kinase-dead mutation in TNIK (K54A) and corresponding mutation in MIG-15 (K50A) are highlighted in red. (F–I) Quantification of overlap between DA8 and DA9 synaptic domains (F and I), DA9 synaptic domain (G), DA8 asynaptic domain (H) in respective mutant backgrounds. Each dot represents measurements from a single animal. Blue bars indicate mean ± SEM. n.s.: not significant; ****p*<0.001; **p*<0.05.

DOI: <https://doi.org/10.7554/eLife.38801.013>

neurons, expression of mutant *mig-15(kd)*, which carries the same mutation at the corresponding amino acid of the dominant-negative TNIK (**Figure 6E**), in DA neurons caused a severe synaptic tiling defect (**Figure 6C, D and I**). Based on these results, we conclude that *mig-15* functions cell autonomously in DA neurons.

***mig-15* inhibits synapse formation**

We observed that DA9-specific expression of *mig-15* under the *mig-13* promoter in *mig-15* mutants often exhibited a shorter synaptic domain compared to wild type (**Figure 6B and G**). So, we speculated that an excess amount of *mig-15* inhibits synapse formation. We tested the effect of *mig-15* overexpression in the wild type background. Strikingly, DA9-specific *mig-15* overexpression in wild type (*mig-15(OE)*) significantly reduced synapse number compared to wild type (**Figure 7A, C and D** and **Figure 7—figure supplement 1**). This reduction occurred without affecting the overall morphology of the DA9 neuron (**Figure 5—figure supplement 1**). Conversely, DA9 synapse number was significantly increased in the *mig-15(rh148)* mutants (**Figure 7B and D** and **Figure 7—figure supplement 1**). *mig-15* overexpression also significantly reduced synapse number in DD-type GABAergic motor neurons (**Figure 7—figure supplement 2**). These results indicate that *mig-15* is a negative regulator of synapse formation. Further, pan-neuronal expression of *mig-15* under the *rab-3* promoter caused severe uncoordinated locomotion in wildtype animals (**Figure 7—figure supplement 3**). These locomotor defects occurred concomitant with significantly reduced GFP::RAB-3 intensity in the dorsal nerve cord in *mig-15* over-expressing animals and without causing significant axon guidance defects (**Figure 7—figure supplement 3**). Taken together, these data indicate that reduced synapse number by *mig-15* overexpression disrupted proper functioning of the motor circuit. Importantly, we observed no significant increase in synapse numbers in *plx-1* or *rap-2* mutants (**Figure 7—figure supplement 1**), suggesting that the role of *mig-15* in negatively regulating synapse number is independent of its role in PLX-1/RAP-2-mediated synaptic tiling (**Figure 8G**).

Rap GTPase and TNIK are well-known actin cytoskeleton regulators (**Lin et al., 2010, 2008; Taira et al., 2004**). Previous studies demonstrated that presynaptic development requires ARP2/3-dependent branched F-actin (**Chia et al., 2012, 2014**). Branched F-actin visualized by GFP::ut-CH (utrophin calponin homology domain) is enriched within the DA9 synaptic domain (**Figure 7E**) (**Chia et al., 2012; Mizumoto and Shen, 2013a**). We predicted that *mig-15* negatively regulates synapse formation by re-organizing branched F-actin at the anterior edge of the synaptic domain. Consistently, we observed longer synaptic F-actin distribution in *rap-2(gk11)* and *mig-15(rh148)* mutants (**Figure 7F, G and I**). While GFP::ut-CH was observed in the posterior asynaptic axonal region or in the dendrite of DA9, synapse formation is likely inhibited by Wnt and Netrin signaling as previously reported (**Klassen and Shen, 2007; Poon et al., 2008**). Conversely, overexpression of *mig-15* in DA9 significantly decreased the length of synaptic F-actin (**Figure 7H and I**). Overexpression of *mig-15* also appeared to decrease the overall amount of synaptic F-actin (**Figure 7H**). This result suggests that *mig-15* inhibits synapse formation by negatively regulating the formation of synaptic F-actin.

***plx-1* and *rap-2* coordinate synaptic tiling border positioning and synapse number**

mig-15(OE) reduced the number of synapses in DA9. As a result, the length of the DA9 synaptic domain was significantly reduced in *mig-15(OE)* animals than in wild type (**Figure 8A and E**). Yet, synaptic tiling is maintained without a significant gap between DA8 and DA9 synaptic domains in *mig-15(OE)* animals, suggesting that the position of synaptic tiling border shifted posteriorly in *mig-15(OE)* animals. Indeed, the length of the posterior asynaptic domain of DA8 was significantly shorter in *mig-15(OE)* animals, indicating that the DA8 synaptic domain expanded posteriorly (**Figure 8D**). The PLX-1::GFP patch at the anterior edge of the DA9 synaptic domain also shifted posteriorly in *mig-15(OE)* animals with reduced synapse number (**Figure 3D**). These results strongly suggest that the PLX-1/RAP-2 signaling pathway may specify the position of the synaptic tiling border according to the available number of synapses in each DA neuron (**Figure 8G**). We propose that synaptic tiling is a mechanism to maintain a uniform distribution of synapses from one class of motor neuron in the nerve cord. Consistently, we found that DA8 synaptic domain did not shift posteriorly when *mig-15* was overexpressed in DA9 of the synaptic tiling mutants, *plx-1* or *rap-2* (**Figure 8B–E**).

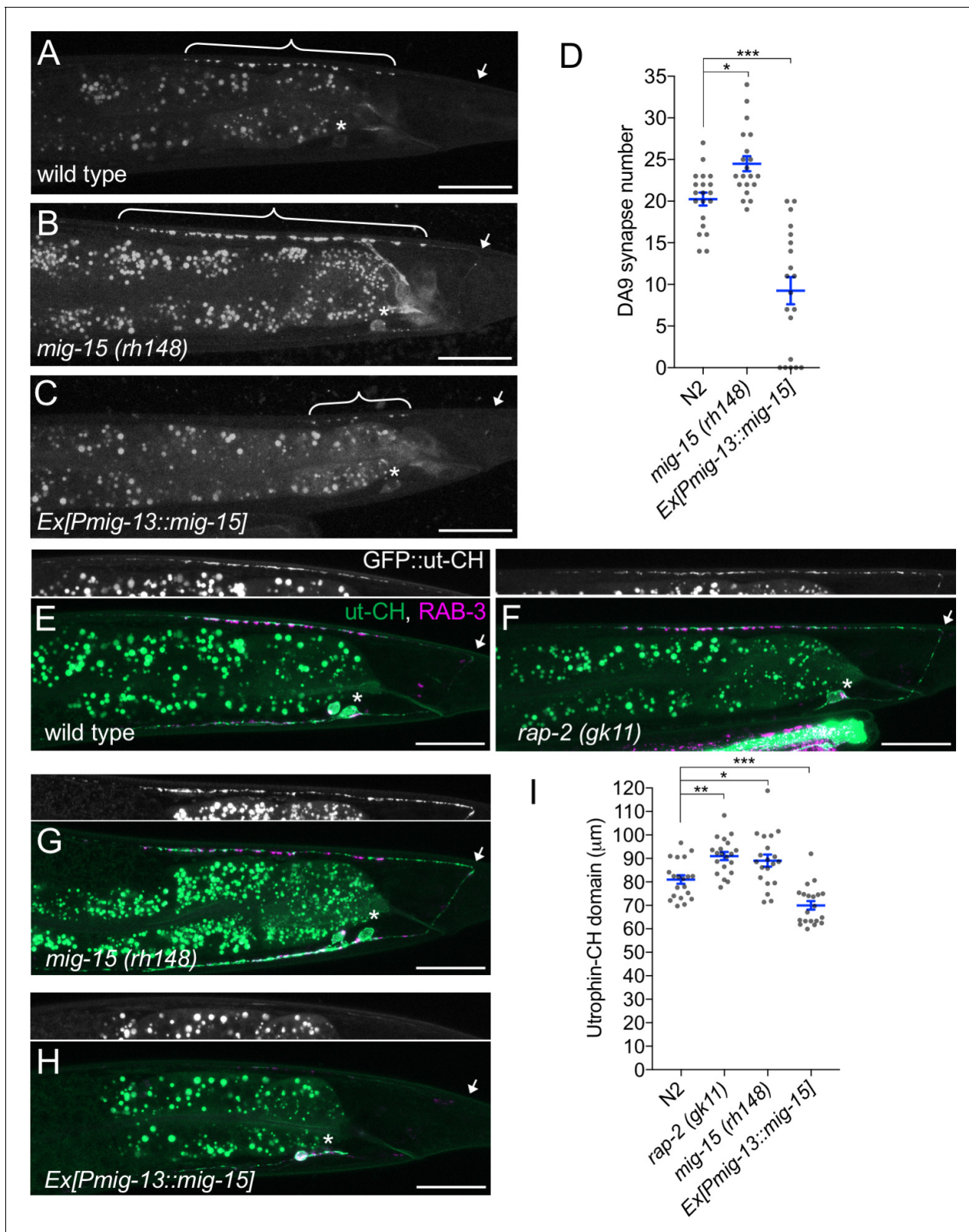


Figure 7. *mig-15* negatively regulates synapse number. (A–C) Representative images of DA9 presynaptic marker, GFP::RAB-3 (*wyls85*), in wild type (A), *mig-15(rh148)* (B) and *mig-15* overexpressing animals (C). Brackets represent DA9 synaptic domain. Asterisks: DA9 cell body. Arrows: dorsal commissure of DA9. Scale bars: 20 μ m. (D) Quantification of DA9 synapse number. Each dot represents measurements from a single animal. Blue bars indicate mean \pm SEM. n.s.: not significant; *** $p < 0.001$; * $p < 0.05$. (E–H) Representative images of synaptic branched F-actin labeled with GFP::ut-CH (*wyls329*) in wild type (E), *rap-2(gk11)* (F), *mig-15(rh148)* (G) and *mig-15* overexpressing animals (H). (I) Quantification of Utrophin-CH domain length. Each dot represents measurements from a single animal. Blue bars indicate mean \pm SEM. n.s.: not significant; *** $p < 0.001$; ** $p < 0.01$; * $p < 0.05$.

Figure 7 continued

wild type (E), *rap-2(gk11)* (F), *mig-15(rh148)* (G) and *mig-15* overexpressing animals (H). (I) Quantification of the length of GFP::ut-CH. Distance from the dorsal commissure to the most anterior and brightest GFP spot was measured. Blue bars indicate mean \pm SEM. n.s.: not significant; *** $p < 0.001$; ** $p < 0.01$, * $p < 0.05$.

DOI: <https://doi.org/10.7554/eLife.38801.014>

The following figure supplements are available for figure 7:

Figure supplement 1. *mig-15* is a negative regulator of synapse formation.

DOI: <https://doi.org/10.7554/eLife.38801.015>

Figure supplement 2. Overexpression of *mig-15* reduces synapse numbers in GABAergic motor neurons.

DOI: <https://doi.org/10.7554/eLife.38801.016>

Figure supplement 3. Reduction of synapses by *mig-15* overexpression caused severe locomotion defects.

DOI: <https://doi.org/10.7554/eLife.38801.017>

This result suggests that DA8 no longer senses the reduction of DA9 synapse number in the synaptic tiling mutants. Synapse number was not different between *mig-15(OE)* and in *rap-2(gk11); mig-15(OE)* animals (**Figure 7—figure supplement 1**), suggesting that *mig-15* is not dependent on the Plexin/Rap2 signaling pathway to inhibit synapse number (**Figure 8G**).

In summary, we demonstrate that synaptic tiling maintains a uniform distribution of synapses from one class of motor neurons along the nerve cord. Further, our results indicate *plx-1* and *rap-2* play critical roles in this process by coordinating the position of the synaptic tiling border.

Discussion

While much is known about the morphogenic triggers for axon guidance and patterned synapse formation, the downstream sequelae of these intracellular effectors have remained unclear. We discovered the role of Rap2 GTPase and TNIK in synapse pattern formation in *C. elegans*. Since Sema/Plexin signaling processes to inhibit synapse formation are well conserved across species, we propose that Sema/Plexin in mammals also utilize Rap2 and TNIK to regulate synapse patterning.

Cell autonomous and non-autonomous functions of Sema/Plexin signaling components

Previously we showed that both *smp-1* and *plx-1* are necessary and sufficient in DA9, which suggests that *smp-1* and *plx-1* act cell-autonomously in DA9 and non-autonomously in DA8 to regulate synaptic tiling. We proposed that Sema/PLX-1 in DA9 send a retrograde signal to DA8 through an unidentified signaling molecule (X) to induce the synaptic tiling pattern in DA8 (**Mizumoto and Shen, 2013a**). However, we found that both *rap-2* and *mig-15* act cell autonomously, since our DA9-specific rescue experiment only rescued the DA9 phenotype, but not the DA8 phenotype. This conclusion is further supported since the synaptic tiling defects of these mutants were fully rescued when both neurons express functional *rap-2* cDNA or *mig-15* genomic DNA. We propose that each neuron utilizes a different set of cell surface proteins but share common intracellular mechanisms to specify synapse patterning. Diverse signaling and cell adhesion molecules, such as atrial natriuretic peptide receptor (NPR) and GPCRs, regulate Rap activity (**Gloerich and Bos, 2011; Birukova et al., 2008; Weissman et al., 2004**). Screening for these potential Rap regulators should identify novel molecules that interact with Sema/Plexin and act in DA9.

Cycling of Rap GTPase activity in synaptic tiling

We showed that proper synapse patterning requires both GDP- and GTP-forms of RAP-2. Considering that PLX-1 regulates the spatial distribution of RAP-2 activity and *mig-15* acts genetically downstream of *plx-1* in synaptic tiling, RAP-2 may also locally regulate MIG-15 (TNIK). While we did not observe a specific subcellular localization of GFP-MIG-15 in DA9 (data not shown), PLX-1 and RAP-2 may instead regulate MIG-15 activity rather than its spatial localization. Further biochemical characterization of MIG-15 regulation by GTP-RAP-2 or GDP-RAP-2 will elucidate the exact functions of RAP-2 in synapse patterning.

Small GTPase activity is regulated by GAP and GEF (Guanine nucleotide exchange factor) proteins. Yet, we did not observe significant synaptic tiling defects in mutants of putative RAP-2 GEFs,

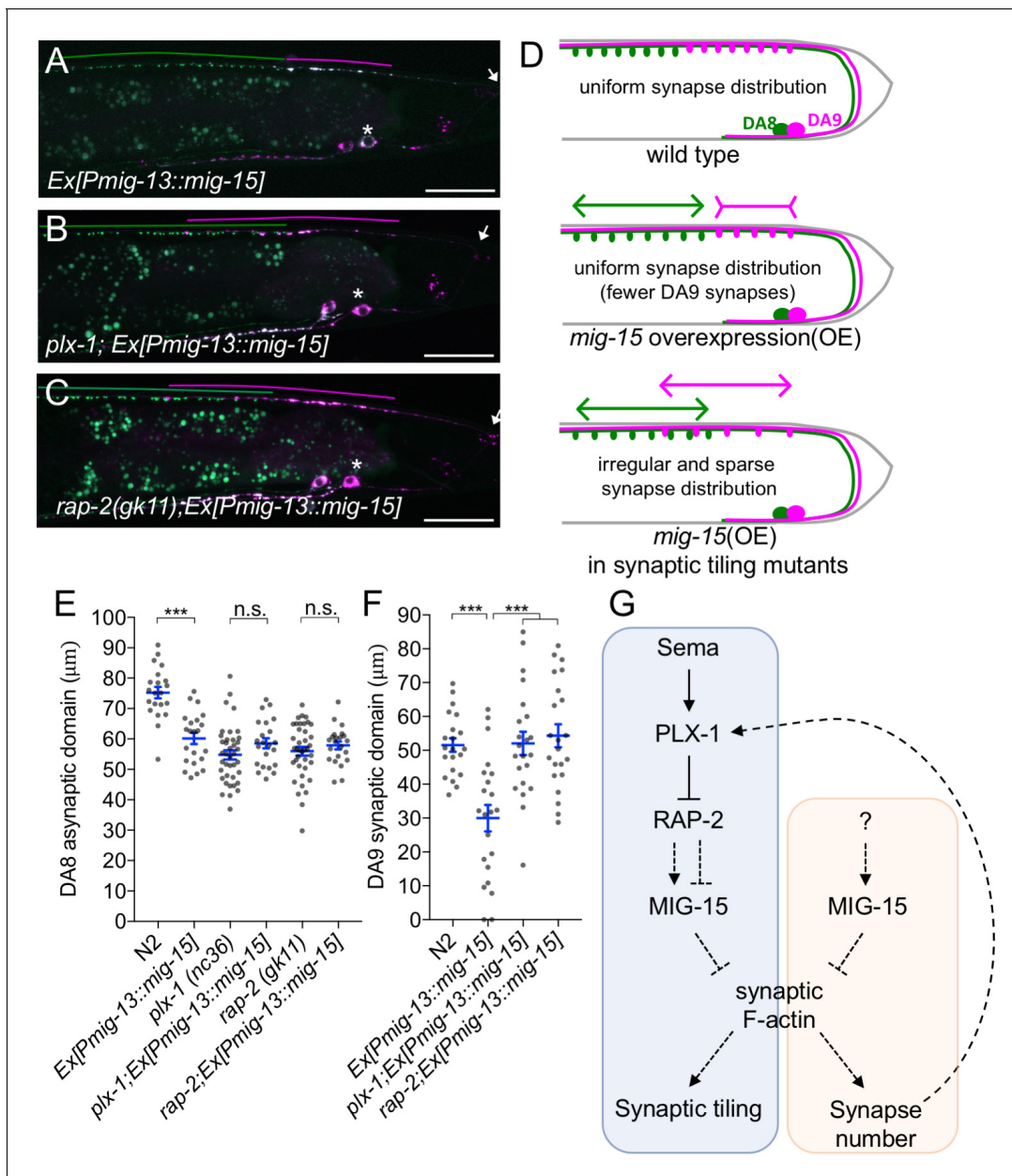


Figure 8. PLX-1/RAP-2 signaling coordinates synapse number and synaptic tiling border. (A–C) Representative images of synaptic tiling marker (*wyls446*) overexpressing *mig-15* in DA9 from wild type (A), *plx-1(nc36)* (B) and *rap-2(gk11)* (C). Synaptic domains of DA8 and DA9 highlighted with green and magenta lines, respectively. Asterisks: DA9 cell body. Arrows: dorsal commissure of DA9. Scale bars: 20 μm . (D) Schematic illustration of synapse distribution in wild type (left), animals overexpressing *mig-15* in DA9 (middle) and synaptic tiling mutants overexpressing *mig-15* in DA9 (right). Arrows indicate the synaptic tiling border. Colored arrows represent expanded or shortened synaptic domain from DA8 (green) and DA9 (magenta). (E) Quantification of the DA8 asynchronous domain. (F) Quantification of the DA9 synaptic domain. Each dot represents measurements from a single animal. Blue bars indicate mean \pm SEM. n.s.: not significant; *** $p < 0.001$. (G) A model of synaptic tiling. PLX-1/RAP-2 signaling controls synaptic tiling via MIG-15, while MIG-15 also plays crucial roles in inhibiting the number of synapses. Solid lines indicate putative direct regulations, dotted lines represent indirect or unknown mode of regulations.

DOI: <https://doi.org/10.7554/eLife.38801.018>

which include *pxf-1(RAPGEF2/6)* and *epac-1(RAPGEF3/4/5)* (data not shown) (Frische et al., 2007; Pellis-van Berkel et al., 2005). We speculate that multiple RapGEFs act redundantly to activate RAP-2 in synaptic tiling.

***mig-15*(TNIK) may integrate multiple inhibitory cues during synapse formation**

mig-15 mutants show a greater degree of overlap between DA8 and DA9 synaptic domains than *plx-1* or *rap-2* mutants. This effect partially occurs from excess synaptogenesis in the posterior synaptic domain of both DA8 and DA9 neurons. Previously, we demonstrated that Wnt morphogens and their receptors, Frizzled, instruct synaptic topographic patterning by locally inhibiting synapse formation. Indeed, synaptic tiling defects in *mig-15* mutants was somewhat similar to the combined effect of *plx-1* and *wnt* mutants (*Mizumoto and Shen, 2013b*). TNIK can act as a positive regulator of the canonical Wnt signaling pathway in colorectal cancer cells (*Mahmoudi et al., 2009; Shitashige et al., 2010*). While we do not know whether the canonical Wnt signaling pathway contributes to local inhibition of synapse formation, we propose that TNIK integrates multiple signaling pathways for precise synapse pattern formation.

In addition to its role in synapse pattern formation, our data indicate that *mig-15* also plays a role as a negative regulator of synapse number. Since neither *plx-1* nor *rap-2* mutants showed a significant increase in synapse number in DA9, *mig-15* may inhibit synapse formation in a different signaling pathway (**Figure 8G**). As we observed a global reduction of synaptic actin staining in animals over-expressing *mig-15*, we propose that *mig-15* controls synapse number by regulating synaptic F-actin.

The exact mechanisms of synaptic actin regulation by TNIK remain undetermined. TNIK could activate the JNK kinase pathway (*Taira et al., 2004; Fu et al., 1999*). The MIG-15/JNK-1 signaling pathway inhibits axonal branch formation in *C. elegans* sensory neurons (*Crawley et al., 2017*). In contrast to these well-established roles of MIG-15/TNIK as an activator of the JNK pathway, we did not observe any synaptic tiling defect nor change in synapse number in *jnk-1* mutant animals (**Figure 5—figure supplement 2** and data not shown). Our results suggest *mig-15* does not inhibit synapse formation through the JNK pathway.

Due to the pleiotropic phenotype of the *mig-15* mutants, our genetic and phenotypic analyses of *mig-15* did not exquisitely reveal the mechanistic relationship between PLX-1 and MIG-15 in synaptic tiling regulation. Further biochemical studies of MIG-15 regulation by Plexin/Rap2 in synaptic tiling will elucidate the molecular mechanisms that underlie the role of MIG-15/TNIK in synapse pattern formation.

Plexin signaling and diseases

Aberrant neuronal wiring underlies many neurological disorders. Not surprisingly, Semaphorin and Plexin genes are associated with various neurodevelopmental disorders and intellectual disabilities, including autism spectrum disorders (ASD) and schizophrenia (*Mah et al., 2006; Gene Discovery Project of Johns Hopkins & the Autism Consortium et al., 2009*). For example, PLXNB1, SEMA3A, SEMA4D and SEMA6C are significantly upregulated in the prefrontal cortices of schizophrenic patients (*Eastwood et al., 2003; Gilbert-Juan et al., 2015*). On the other hand, non-synonymous variations in the Sema3D gene had a significant protective effect against developing schizophrenia (*Fujii et al., 2011*). More recent work showed that loss of Sema5A/PlexA2 signaling induces excess excitatory synapse formation in granule cells, which caused ASD-like behavioural defects in mice (*Duan et al., 2014*).

Similar to Sema/Plexin signaling, TNIK is also associated with various neurological disorders, including schizophrenia and intellectual disabilities (*Anazi et al., 2016; Potkin et al., 2010*). TNIK can also physically bind and act with DISC1 (Disrupted in Schizophrenia 1) to regulate synaptic composition (*Wang et al., 2011*). So, we propose that the Sema/Plexin/Rap2/TNIK signaling pathway plays a critical role to precisely define synaptic connections and its disruption may induce serious neurological disorders.

Interestingly, SNPs in Plexin genes are also associated with extremely high IQ (*Spain et al., 2016*). Recent work suggests that loss of PlexinA1 confers better motor control in rodents due to increased synaptic connectivity in the corticospinal cord (*Gu et al., 2017*). Further studies on the Plexin/Rap2/TNIK signaling pathway in synapse map formation, as presented here, will likely reveal the genetic basis of these disorders and conditions.

Materials and methods

Key resources table

Reagent type (species) or resource	Designation	Source or reference	Identifiers	Additional information
Gene (<i>C. elegans</i>)	rap-2	NA	C25D7.7	
Gene (<i>C. elegans</i>)	plx-1	NA	Y55F3AL.1	
Gene (<i>C. elegans</i>)	mig-15	NA	ZC504.4	
Strain, strain background (<i>C. elegans</i>)	rap-2(gk11)	<i>C. elegans</i> stock center (CGC)	VC14	
Strain, strain background (<i>C. elegans</i>)	mig-15(rh148)	<i>C. elegans</i> stock center (CGC)	NJ490	
Strain, strain background (<i>C. elegans</i>)	plx-1(nc36)	<i>C. elegans</i> stock center (CGC)	ST36	
Strain, strain background (<i>C. elegans</i>)	rap-2(miz18)	This study	UJ401	G12V mutant
Strain, strain background (<i>C. elegans</i>)	rap-2(miz19)	This study	UJ402	S17A mutant
Strain, strain background (<i>C. elegans</i>)	wyls446	This study	TV14517	synaptic tiling marker
Strain, strain background (<i>C. elegans</i>)	mizls19	This study	UJ397	Rap2 FRET sensor strain

Strains

All *C. elegans* strains were derived from Bristol N2 and raised on OP50 *Escherichia coli*-seeded nematode growth medium (NGM) plates at 20C and maintained as described previously (Brenner, 1974). The following mutants were used in this study: *unc-104(e1265)II*, *plx-1(nc36)IV*, *rap-1(pk2082)IV*, *rap-3(gk3975)IV*, *jnk-1(gk7)IV*, *rap-2(gk11)V*, *rap-2(miz16)V*, *rap-2(miz17)V*, *rap-2(miz18)V*, *rap-2(miz19)V*, *rap-2(miz20)V*, *mig-15(rh148)X*, *mig-15(rh80)X*, *mig-15(rh326)X*.

CRISPR/Cas9 genome editing

rap-2(miz16)V, *rap-2(miz17)V*, *rap-2(miz18)V*, *rap-2(miz19)V*, *rap-2(miz20)V* were generated using Co-CRISPR method (Kim et al., 2014). *unc-22* or *dpy-10* co-CRISPR markers were used for selecting candidate animals (Kim et al., 2014; Arribere et al., 2014). Vectors for sgRNA and Cas9 were obtained from Addgene (Plasmid ID: 46169 and 46168, respectively) (Friedland et al., 2013). The *rap-2* guide RNA sequence (5' – gTAGTGGAGGTGTCGAAAAT-3') was designed using MIT CRISPR design tool (crispr.mit.edu:8079) and inserted into sgRNA vector using Q5 Site-Directed Mutagenesis kit (NEB). Repair templates with either G12V (*miz17* and *miz18*) and S17A (*miz19* and *miz20*) mutation were generated by PCR with primer sets carrying corresponding mutations (see supplemental Experimental Procedures). Synonymous mutations were also introduced in the sgRNA recognition sequence to avoid Cas9 recruitment to the edited genome. PCR products were cloned into *EcoRI* site of the pBluescript SK(+) vector. Synthesized double-stranded DNA (GeneArt, Thermo Fisher) was used as a repair template for generating *rap-2(miz16)* mutant.

Plasmid constructions

C. elegans expression clones were made in a derivative of pPD49.26 (A. Fire), the pSM vector (kind gift from S. McCarroll and C. I. Bargmann). Primer sets used in this study are listed in the Supplemental Experimental Procedures. The following constructs were used and transgenes were generated using standard microinjection method (Mello et al., 1991): *wyls446* (*Punc-4::2xGFP-rab-3*; *Pmig-13::mCherry-rab-3*; *Podr-1::RFP*), *wyls85* (*Pitr-1::GFP-rab-3*; *Podr-1::RFP*), *wyls442* (*Pflp-13::2xGFP-rab-3*; *Pplx-2::mCherry-rab-3*; *Podr-1::RFP*), *wyls320* (*Pitr-1::plx-1::GFP*; *Pmig-13::mCherry::rab-3*; *Podr-1::GFP*), *wyls329* (*Pmig-13::GFP-ut-CH*; *Pmig-13::mCherry::rab-3*; *Podr-1::GFP*), *wyls524* (*Punc-4::2xGFP-rab-3*; *Pmig-13::mCherry-rab-3*; *Podr-1::RFP*), *wyls685* (*Pmig-13::*

mCherry::rab-3; Pmig-13::GFPnovo2::cla-1; Podr-1::GFP) *mizls1* (*Pitr-1::GFPnovo2-CAAX; Pvha-6::zif-1; Pitr-1::mCherry::rab-3; Podr-1::GFP*), *mizls19* (*Pmig-13::eGFP::hRap2a; Pmig-13::mRFP-RalGDS (RBD)-mRFP; Podr-1::GFP*), *mizls33* (*Prab-3::mig-15; Podr-1::GFP*), *jls682* (*Prab-3::GFP::rab-3; lin-15 (+)*), *wyEx5445* (*Prap-1::GFP; Punc-4::myr-mCherry; Podr-1::RFP*), *wyEx5464* (*Prap-2::GFP; Punc-4::myr-mCherry; Podr-1::RFP*), *mizEx194* (*Prap-3::GFP; Pmig-13::myr-mCherry; Podr-1::RFP*), *mizEx165* (*Phlh-1::rap-2; Podr-1::GFP*), *mizEx164* (*Punc-129::rap-2; Podr-1::GFP*), *mizEx174* (*Punc-4c::rap-2; Podr-1::GFP*), *mizEx157* (*Pmig-13::rap-2; Podr-1::GFP*), *mizEx156* (*Punc-4c::hRap2a; Podr-1::GFP*), *mizEx177* (*Punc-4c::rap-1; Podr-1::GFP*), *mizEx151* (*Pmig-13::mig-15; Podr-1::GFP*), *mizEx147* (*Punc-4c::mig-15; Podr-1::GFP*), *mizEx153* (Δ pSM*mig-15; Podr-1::GFP*), *mizEx178* (*Punc-4c::mig-15(K50A); Podr-1::GFP*), *mizEx173* (*Punc-4c::rap-2(G12V); Podr-1::GFP*), *mizEx179* (*Pflp-13::mig-15; Podr-1::GFP*), *mizEx170* (*Pmig-13::mig-15; Podr-1::GFP*), *mizEx197* (*Pmig-13::mig-15; Podr-1::GFP*), *mizEx210* (*Pmig-13::mig-15; Podr-1::RFP*), *mizEx257* (*Prab-3::GFP; Prab-3::mCherry::rab-3, Podr-1::mScarlet::CAAX*), *mizEx272* (*Podr-1::GFP; Pmig-13::unc-10::TdTomato*), *mizEx309* (*Pmig-13::plx-1 (RA); Podr-1::RFP*), *mizEx312* (*Pmig-13::plx-1(Δ sema); Podr-1::RFP*), *mizEx314* (*Pmig-13::plx-1; Podr-1::RFP*).

Cloning of *rap-1*, *rap-2* and *mig-15*

cDNAs of *rap-1* and *rap-2* were obtained from cDNA library prepared from N2 RNA. Trizol (Invitrogen) was used to purify total RNA from N2, and the SuperScript III First-Strand Synthesis System for RT-PCR (Invitrogen) was used for the reverse-transcription. *mig-15* genomic DNA was amplified from the N2 genomic DNA purified using GeneJET Genomic DNA Purification Kit (Thermo Scientific). Phusion (NEB) or Q5 (NEB) DNA polymerases were used for all PCR reactions for amplifying cDNA and genomic DNA fragments. Amplified fragments were cloned into the *Ascl* and *KpnI* sites of pSM vector using SLICE method (Motohashi, 2015), Gibson assembly (Gibson et al., 2009) or T4 ligase (NEB). List of primers used in this study is available in the Supplemental Experimental Procedures.

Confocal microscopy

Images of fluorescently tagged fusion proteins were captured in live *C. elegans* using a Zeiss LSM800 confocal microscope (Carl Zeiss, Germany). Worms were immobilized on 2% agarose pad using a mixture of 7.5 mM levamisole (Sigma-Aldrich) and 0.225M BDM (2,3-butanedione monoxime) (Sigma-Aldrich). Images were analyzed with Zen software (Carl Zeiss) or Image J (NIH, USA). Definition of each parameter is as follows (Mizumoto and Shen, 2013a): DA8/9 overlap: a distance between the most anterior DA9 synapse and the most posterior DA8 synapse, DA8 synaptic domain: a distance from commissure to the most posterior DA8 synapse, DA9 synaptic domain: a distance between the most anterior and posterior DA9 synapses. Middle L4 (judged by the stereotyped shape of developing vulva) animals were used for quantification. Averages were taken from at least 20 samples. For GFP::Utrrophin-CH, we measured the length from the posterior end of dorsal axon to the anterior end of GFP::Utrrophin-CH domain. For each marker strain, the same imaging setting (laser power, gain pinhole) and image processing were used for comparing different genotypes.

Two-photon FLIM-FRET experiment

Expression vector for cultured cells (pCI-eGFP-hRap2a, pCI-eGFP-RAP-1, pCI-eGFP-RAP-2, pCI-eGFP-RAP-2(G12V), pCI-eGFP-RAP-2(S17A)) were generated by replacing Ras in pCI-eGFP-Ras (Yasuda et al., 2006) with hRap2a and *rap-2* cDNAs with *XhoI* and *BamHI*. pCI-mRFP-RalGDS-mRFP plasmid is a kind gift from Dr. Yasuda. Rap2 and FRET sensor plasmids were mixed in 1:2 ratio and transfected into HeLa cells using Lipofectamine 3000 (ThermoFisher). FLIM was conducted 24 hr after transfection. For expression of FRET sensor in the DA9 neuron, each fusion protein constructs were cloned into *Ascl* and *KpnI* sites of the pSM vector containing *mig-13* promoter using SLICE method.

A custom-made two-photon fluorescence lifetime imaging microscope was used as described elsewhere (Murakoshi et al., 2011). Briefly, EGFP-Rap2a was excited with a Ti-sapphire laser (Mai Tai; Spectra-Physics) tuned to 920 nm. The X and Y scanning galvano mirrors (6210 hr; Cambridge Technology) were controlled with ScanImage software (Pologruto et al., 2003). EGFP photon signals

were collected an objective lens (60×, 1.0 NA; Olympus) and a photomultiplier tube (H7422-40p; Hamamatsu) placed after a dichroic mirror (FF553-SDi01; Semrock) and emission filter (FF01-510/84; Semrock). A fluorescence lifetime curve was recorded by a time-correlated single-photon-counting board (SPC-150; Becker and Hickl) controlled with the software described previously (Yasuda et al., 2006). For construction of a fluorescence lifetime image, the mean fluorescence lifetime values (τ_m) in each pixel were translated into a color-coded image. We quantified free EGFP-Rap2a and EGFP-Rap2a undergoing FRET (binding fraction) as described elsewhere (Yasuda et al., 2006). Briefly, we calculated the proportion of EGFP undergoing FRET in individual ROIs using the following formula:

$$P_{\text{FRET}} = \frac{\tau_{\text{free}}(\tau_{\text{free}} - \tau_m)}{(\tau_{\text{free}} - \tau_{\text{FRET}})(\tau_{\text{free}} + \tau_{\text{FRET}} - \tau_m)} P_{\text{FRET}} = \frac{\tau_{\text{free}}(\tau_{\text{free}} - \tau_m)}{(\tau_{\text{free}} - \tau_{\text{FRET}})(\tau_{\text{free}} + \tau_{\text{FRET}} - \tau_m)} \quad (1)$$

where τ_{free} and τ_{FRET} are the fluorescence lifetime of free EGFP and EGFP undergoing FRET, respectively.

Statistics

Prism (GraphPad) software was used for statistical analysis. One-way ANOVA was done and corrected for multiple comparisons with posthoc Tukey's multiple comparisons tests done between all genotypes. Student's t-test was used for pairwise comparison. Sample numbers were pre-determined before conducting statistical analyses.

Supplemental experimental procedures

The method for qRT-PCR and sequences of primers and repair templates used in this study are available in **Supplementary file 1**.

Acknowledgements

We are grateful to Donald Moerman and his lab members for generating *rap-3* mutant strain, providing other mutant strains, sharing reagents and for general discussions. We also thank Ryohei Yasuda for FRET sensor plasmids, Hiroshi Kawabe for human Rap2a cDNA, Richard Ikegami for *plx-2* promoter construct, Harald Hutter and Peri Kurshan for sharing strains, May Dang-Lawson and Michael Gold for unpublished biochemical experiments, Lisa Fernando for the technical support, all Mizumoto lab members and general discussions, Kang Shen, Shaul Yogev and Maulik Patel for comments on the manuscript. Some strains used in this study were obtained from the CGC, which is funded by NIH Office of Research Infrastructure Programs (P40 OD010440) and *C. elegans* gene knock out consortium. Mizumoto Lab is funded by HFSP (CDA-00004/2014), CIHR (PJT-148667), NSERC (RGPIN-2015-04022), CFI-JELF (34722) and Tomizawa Jun-ichi and Keiko Fund for Young Scientist. KM is a recipient of Canada Research Chair and Michael Smith Foundation for Health Research Scholar.

Additional information

Funding

Funder	Grant reference number	Author
Human Frontier Science Program	CDA-00004/2014	Kota Mizumoto
Canadian Institutes of Health Research	PJT-148667	Kota Mizumoto
Natural Sciences and Engineering Research Council of Canada	RGPIN-2015-04022	Kota Mizumoto
Canada Research Chairs		Kota Mizumoto
Michael Smith Foundation for Health Research	16869	Kota Mizumoto

Tomizawa Jun-ichi and Keiko
Fund of Molecular Biology So-
ciety of Japan for Young
Scientists

Kota Mizumoto

Canada Foundation for Inno- 34722
vation

Kota Mizumoto

The funders had no role in study design, data collection and interpretation, or the decision to submit the work for publication.

Author contributions

Xi Chen, Formal analysis, Investigation, Visualization; Akihiro CE Shibata, Ardalan Hendi, Mizuki Kurashina, Ethan Fortes, Formal analysis, Validation, Investigation, Visualization, Writing—review and editing; Nicholas L Weiling, Investigation, Writing—review and editing; Brian A MacVicar, Resources, Supervision; Hideji Murakoshi, Resources, Supervision, Validation, Investigation, Writing—review and editing; Kota Mizumoto, Conceptualization, Data curation, Formal analysis, Supervision, Funding acquisition, Validation, Investigation, Visualization, Writing—original draft, Writing—review and editing

Author ORCIDs

Brian A MacVicar  <http://orcid.org/0000-0003-4596-4623>

Kota Mizumoto  <http://orcid.org/0000-0001-8091-4483>

Decision letter and Author response

Decision letter <https://doi.org/10.7554/eLife.38801.023>

Author response <https://doi.org/10.7554/eLife.38801.024>

Additional files

Supplementary files

- Supplementary file 1. Supplementary experimental procedures.

DOI: <https://doi.org/10.7554/eLife.38801.019>

- Transparent reporting form

DOI: <https://doi.org/10.7554/eLife.38801.020>

Data availability

All data generated or analyzed during this study are included in the manuscript and supporting files.

References

- Anazi S, Shamseldin HE, AlNaqeb D, Abouelhoda M, Monies D, Salih MA, Al-Rubeaan K, Alkuraya FS. 2016. A null mutation in TNIK defines a novel locus for intellectual disability. *Human Genetics* **135**:773–778. DOI: <https://doi.org/10.1007/s00439-016-1671-9>, PMID: 27106596
- Arribere JA, Bell RT, Fu BX, Artiles KL, Hartman PS, Fire AZ. 2014. Efficient marker-free recovery of custom genetic modifications with CRISPR/Cas9 in *Caenorhabditis elegans*. *Genetics* **198**:837–846. DOI: <https://doi.org/10.1534/genetics.114.169730>, PMID: 25161212
- Birukova AA, Zagranichnaya T, Alekseeva E, Bokoch GM, Birukov KG. 2008. Epac/Rap and PKA are novel mechanisms of ANP-induced Rac-mediated pulmonary endothelial barrier protection. *Journal of Cellular Physiology* **215**:715–724. DOI: <https://doi.org/10.1002/jcp.21354>, PMID: 18064650
- Brenner S. 1974. The genetics of *Caenorhabditis elegans*. *Genetics* **77**:71–94. PMID: 4366476
- Chapman JO, Li H, Lundquist EA. 2008. The MIG-15 NIK kinase acts cell-autonomously in neuroblast polarization and migration in *C. elegans*. *Developmental Biology* **324**:245–257. DOI: <https://doi.org/10.1016/j.ydbio.2008.09.014>, PMID: 18840424
- Chia PH, Chen B, Li P, Rosen MK, Shen K. 2014. Local F-actin network links synapse formation and axon branching. *Cell* **156**:208–220. DOI: <https://doi.org/10.1016/j.cell.2013.12.009>, PMID: 24439377
- Chia PH, Patel MR, Shen K. 2012. NAB-1 instructs synapse assembly by linking adhesion molecules and F-actin to active zone proteins. *Nature Neuroscience* **15**:234–242. DOI: <https://doi.org/10.1038/nn.2991>, PMID: 22231427

- Crawley O**, Giles AC, Desbois M, Kashyap S, Birnbaum R, Grill B. 2017. A MIG-15/JNK-1 MAP kinase cascade opposes RPM-1 signaling in synapse formation and learning. *PLoS Genetics* **13**:e1007095. DOI: <https://doi.org/10.1371/journal.pgen.1007095>, PMID: 29228003
- Dabrowski A**, Terauchi A, Strong C, Umemori H. 2015. Distinct sets of FGF receptors sculpt excitatory and inhibitory synaptogenesis. *Development* **142**:1818–1830. DOI: <https://doi.org/10.1242/dev.115568>, PMID: 25926357
- Dabrowski A**, Umemori H. 2016. Buttressing a balanced brain: target-derived FGF signaling regulates excitatory/inhibitory tone and adult neurogenesis within the maturing hippocampal network. *Neurogenesis* **3**:e1168504. DOI: <https://doi.org/10.1080/23262133.2016.1168504>, PMID: 27605441
- Dalpé G**, Brown L, Culotti JG. 2005. Vulva morphogenesis involves attraction of plexin 1-expressing primordial vulva cells to semaphorin 1a sequentially expressed at the vulva midline. *Development* **132**:1387–1400. DOI: <https://doi.org/10.1242/dev.01694>, PMID: 15716342
- Dalpé G**, Zhang LW, Zheng H, Culotti JG. 2004. Conversion of cell movement responses to Semaphorin-1 and Plexin-1 from attraction to repulsion by lowered levels of specific RAC GTPases in *C. elegans*. *Development* **131**:2073–2088. DOI: <https://doi.org/10.1242/dev.01063>, PMID: 15073148
- Duan Y**, Wang SH, Song J, Mironova Y, Ming GL, Kolodkin AL, Giger RJ. 2014. Semaphorin 5A inhibits synaptogenesis in early postnatal- and adult-born hippocampal dentate granule cells. *eLife* **3**:e04390. DOI: <https://doi.org/10.7554/eLife.04390>, PMID: 25313870
- Eastwood SL**, Law AJ, Everall IP, Harrison PJ. 2003. The axonal chemorepellant semaphorin 3A is increased in the cerebellum in schizophrenia and may contribute to its synaptic pathology. *Molecular Psychiatry* **8**:148–155. DOI: <https://doi.org/10.1038/sj.mp.4001233>, PMID: 12610647
- Epstein JA**, Aghajanian H, Singh MK. 2015. Semaphorin signaling in cardiovascular development. *Cell Metabolism* **21**:163–173. DOI: <https://doi.org/10.1016/j.cmet.2014.12.015>, PMID: 25651171
- Feng G**, Laskowski MB, Feldheim DA, Wang H, Lewis R, Frisen J, Flanagan JG, Sanes JR. 2000. Roles for ephrins in positionally selective synaptogenesis between motor neurons and muscle fibers. *Neuron* **25**:295–306. DOI: [https://doi.org/10.1016/S0896-6273\(00\)80895-8](https://doi.org/10.1016/S0896-6273(00)80895-8), PMID: 10719886
- Friedland AE**, Tzur YB, Esvelt KM, Colaiácovo MP, Church GM, Calarco JA. 2013. Heritable genome editing in *C. elegans* via a CRISPR-Cas9 system. *Nature Methods* **10**:741–743. DOI: <https://doi.org/10.1038/nmeth.2532>, PMID: 23817069
- Frische EW**, Pellis-van Berkel W, van Haaften G, Cuppen E, Plasterk RH, Tijsterman M, Bos JL, Zwartkruis FJ. 2007. RAP-1 and the RAL-1/exocyst pathway coordinate hypodermal cell organization in *Caenorhabditis elegans*. *The EMBO Journal* **26**:5083–5092. DOI: <https://doi.org/10.1038/sj.emboj.7601922>, PMID: 17989692
- Fu CA**, Shen M, Huang BC, Lasaga J, Payan DG, Luo Y. 1999. TNIK, a novel member of the germinal center kinase family that activates the c-Jun N-terminal kinase pathway and regulates the cytoskeleton. *The Journal of Biological Chemistry* **274**:30729–30766. DOI: <https://doi.org/10.1074/jbc.274.43.30729>, PMID: 10521462
- Fu Z**, Lee SH, Simonetta A, Hansen J, Sheng M, Pak DT. 2007. Differential roles of Rap1 and Rap2 small GTPases in neurite retraction and synapse elimination in hippocampal spiny neurons. *Journal of Neurochemistry* **100**:118–131. DOI: <https://doi.org/10.1111/j.1471-4159.2006.04195.x>, PMID: 17227435
- Fujii T**, Nakao F, Shibata Y, Shioi G, Kodama E, Fujisawa H, Takagi S. 2002. *Caenorhabditis elegans* PlexinA, PLX-1, interacts with transmembrane semaphorins and regulates epidermal morphogenesis. *Development* **129**:2053–2063. PMID: 11959816
- Fujii T**, Uchiyama H, Yamamoto N, Hori H, Tatsumi M, Ishikawa M, Arima K, Higuchi T, Kunugi H. 2011. Possible association of the semaphorin 3D gene (SEMA3D) with schizophrenia. *Journal of Psychiatric Research* **45**:47–53. DOI: <https://doi.org/10.1016/j.jpsychires.2010.05.004>, PMID: 20684831
- Gene Discovery Project of Johns Hopkins & the Autism Consortium**, Weiss LA, Arking DE, Daly MJ, Chakravarti A. 2009. A genome-wide linkage and association scan reveals novel loci for autism. *Nature* **461**:802–808. DOI: <https://doi.org/10.1038/nature08490>, PMID: 19812673
- Gibson DG**, Young L, Chuang RY, Venter JC, Hutchison CA, Smith HO. 2009. Enzymatic assembly of DNA molecules up to several hundred kilobases. *Nature Methods* **6**:343–345. DOI: <https://doi.org/10.1038/nmeth.1318>, PMID: 19363495
- Gilabert-Juan J**, Sáez AR, Lopez-Campos G, Sebastián-Ortega N, González-Martínez R, Costa J, Haro JM, Callado LF, Meana JJ, Nacher J, Sanjuán J, Moltó MD. 2015. Semaphorin and plexin gene expression is altered in the prefrontal cortex of schizophrenia patients with and without auditory hallucinations. *Psychiatry Research* **229**:850–857. DOI: <https://doi.org/10.1016/j.psychres.2015.07.074>, PMID: 26243375
- Gloerich M**, Bos JL. 2011. Regulating rap small G-proteins in time and space. *Trends in Cell Biology* **21**:615–623. DOI: <https://doi.org/10.1016/j.tcb.2011.07.001>, PMID: 21820312
- Gloerich M**, ten Klooster JP, Vliem MJ, Koorman T, Zwartkruis FJ, Clevers H, Bos JL. 2012. Rap2A links intestinal cell polarity to brush border formation. *Nature Cell Biology* **14**:793–801. DOI: <https://doi.org/10.1038/ncb2537>, PMID: 22797597
- Gu Z**, Kalambogias J, Yoshioka S, Han W, Li Z, Kawasawa YI, Pochareddy S, Li Z, Liu F, Xu X, Wijeratne HRS, Ueno M, Blatz E, Salomone J, Kumanogoh A, Rasin MR, Gebelein B, Weirauch MT, Sestan N, Martin JH, et al. 2017. Control of species-dependent cortico-motoneuronal connections underlying manual dexterity. *Science* **357**:400–404. DOI: <https://doi.org/10.1126/science.aan3721>, PMID: 28751609
- Hota PK**, Buck M. 2012. Plexin structures are coming: opportunities for multilevel investigations of semaphorin guidance receptors, their cell signaling mechanisms, and functions. *Cellular and Molecular Life Sciences* **69**:3765–3805. DOI: <https://doi.org/10.1007/s00018-012-1019-0>, PMID: 22744749

- Hussain NK**, Hsin H, Haganir RL, Sheng M. 2010. MINK and TNIK differentially act on Rap2-mediated signal transduction to regulate neuronal structure and AMPA receptor function. *Journal of Neuroscience* **30**:14786–14794. DOI: <https://doi.org/10.1523/JNEUROSCI.4124-10.2010>, PMID: 21048137
- Ikegami R**, Zheng H, Ong SH, Culotti J. 2004. Integration of semaphorin-2A/MAB-20, ephrin-4, and UNC-129 TGF-beta signaling pathways regulates sorting of distinct sensory rays in *C. elegans*. *Developmental Cell* **6**: 383–395. DOI: [https://doi.org/10.1016/S1534-5807\(04\)00057-7](https://doi.org/10.1016/S1534-5807(04)00057-7), PMID: 15030761
- Inaki M**, Yoshikawa S, Thomas JB, Aburatani H, Nose A. 2007. Wnt4 is a local repulsive cue that determines synaptic target specificity. *Current Biology* **17**:1574–1579. DOI: <https://doi.org/10.1016/j.cub.2007.08.013>, PMID: 17764943
- Kawabe H**, Neeb A, Dimova K, Young SM, Takeda M, Katsurabayashi S, Mitkovski M, Malakhova OA, Zhang DE, Umikawa M, Kariya K, Goebbels S, Nave KA, Rosenmund C, Jahn O, Rhee J, Brose N. 2010. Regulation of Rap2A by the ubiquitin ligase Nedd4-1 controls neurite development. *Neuron* **65**:358–372. DOI: <https://doi.org/10.1016/j.neuron.2010.01.007>, PMID: 20159449
- Kayser MS**, Nolt MJ, Dalva MB. 2008. EphB receptors couple dendritic filopodia motility to synapse formation. *Neuron* **59**:56–69. DOI: <https://doi.org/10.1016/j.neuron.2008.05.007>, PMID: 18614029
- Kim H**, Ishidate T, Ghanta KS, Seth M, Conte D, Shirayama M, Mello CC. 2014. A co-CRISPR strategy for efficient genome editing in *Caenorhabditis elegans*. *Genetics* **197**:1069–1080. DOI: <https://doi.org/10.1534/genetics.114.166389>, PMID: 24879462
- Klassen MP**, Shen K. 2007. Wnt signaling positions neuromuscular connectivity by inhibiting synapse formation in *C. elegans*. *Cell* **130**:704–716. DOI: <https://doi.org/10.1016/j.cell.2007.06.046>, PMID: 17719547
- Kolodkin AL**, Matthes DJ, Goodman CS. 1993. The semaphorin genes encode a family of transmembrane and secreted growth cone guidance molecules. *Cell* **75**:1389–1399. DOI: [https://doi.org/10.1016/0092-8674\(93\)90625-Z](https://doi.org/10.1016/0092-8674(93)90625-Z), PMID: 8269517
- Kolodkin AL**, Matthes DJ, O'Connor TP, Patel NH, Admon A, Bentley D, Goodman CS. 1992. Fasciclin IV: sequence, expression, and function during growth cone guidance in the grasshopper embryo. *Neuron* **9**:831–845. DOI: [https://doi.org/10.1016/0896-6273\(92\)90237-8](https://doi.org/10.1016/0896-6273(92)90237-8), PMID: 1418998
- Lin KB**, Freeman SA, Gold MR. 2010. Rap GTPase-mediated adhesion and migration: a target for limiting the dissemination of B-cell lymphomas? *Cell Adhesion & Migration* **4**:327–332. DOI: <https://doi.org/10.4161/cam.4.3.11114>, PMID: 20212359
- Lin KB**, Freeman SA, Zabetian S, Brugger H, Weber M, Lei V, Dang-Lawson M, Tse KW, Santamaria R, Batista FD, Gold MR. 2008. The rap GTPases regulate B cell morphology, immune-synapse formation, and signaling by particulate B cell receptor ligands. *Immunity* **28**:75–87. DOI: <https://doi.org/10.1016/j.immuni.2007.11.019>, PMID: 18191594
- Liu Z**, Fujii T, Nukazuka A, Kurokawa R, Suzuki M, Fujisawa H, Takagi S. 2005. *C. elegans* PlexinA PLX-1 mediates a cell contact-dependent stop signal in vulval precursor cells. *Developmental Biology* **282**:138–151. DOI: <https://doi.org/10.1016/j.ydbio.2005.03.002>, PMID: 15936335
- Mah S**, Nelson MR, Delisi LE, Reneland RH, Markward N, James MR, Nyholt DR, Hayward N, Handoko H, Mowry B, Kammerer S, Braun A. 2006. Identification of the semaphorin receptor PLXNA2 as a candidate for susceptibility to schizophrenia. *Molecular Psychiatry* **11**:471–478. DOI: <https://doi.org/10.1038/sj.mp.4001785>, PMID: 16402134
- Mahmoudi T**, Li VS, Ng SS, Taouatas N, Vries RG, Mohammed S, Heck AJ, Clevers H. 2009. The kinase TNIK is an essential activator of Wnt target genes. *The EMBO Journal* **28**:3329–3340. DOI: <https://doi.org/10.1038/emboj.2009.285>, PMID: 19816403
- Matthes DJ**, Sink H, Kolodkin AL, Goodman CS. 1995. Semaphorin II can function as a selective inhibitor of specific synaptic arborizations. *Cell* **81**:631–639. DOI: [https://doi.org/10.1016/0092-8674\(95\)90084-5](https://doi.org/10.1016/0092-8674(95)90084-5), PMID: 7758117
- Mello CC**, Kramer JM, Stinchcomb D, Ambros V. 1991. Efficient gene transfer in *C. elegans*: extrachromosomal maintenance and integration of transforming sequences. *The EMBO Journal* **10**:3959–4029. PMID: 1935914
- Mizumoto K**, Shen K. 2013a. Interaxonal interaction defines tiled presynaptic innervation in *C. elegans*. *Neuron* **77**:655–666. DOI: <https://doi.org/10.1016/j.neuron.2012.12.031>, PMID: 23439119
- Mizumoto K**, Shen K. 2013b. Two Wnts instruct topographic synaptic innervation in *C. elegans*. *Cell Reports* **5**: 389–396. DOI: <https://doi.org/10.1016/j.celrep.2013.09.011>, PMID: 24139806
- Motohashi K**. 2015. A simple and efficient seamless DNA cloning method using SLiCE from *Escherichia coli* laboratory strains and its application to SLiP site-directed mutagenesis. *BMC Biotechnology* **15**:47. DOI: <https://doi.org/10.1186/s12896-015-0162-8>, PMID: 26037246
- Murakoshi H**, Wang H, Yasuda R. 2011. Local, persistent activation of rho GTPases during plasticity of single dendritic spines. *Nature* **472**:100–104. DOI: <https://doi.org/10.1038/nature09823>, PMID: 21423166
- Nakao F**, Hudson ML, Suzuki M, Peckler Z, Kurokawa R, Liu Z, Gengyo-Ando K, Nukazuka A, Fujii T, Suto F, Shibata Y, Shioi G, Fujisawa H, Mitani S, Chisholm AD, Takagi S. 2007. The PLEXIN PLX-2 and the ephrin EFN-4 have distinct roles in MAB-20/Semaphorin 2A signaling in *Caenorhabditis elegans* morphogenesis. *Genetics* **176**:1591–1607. DOI: <https://doi.org/10.1534/genetics.106.067116>, PMID: 17507686
- Negishi M**, Oinuma I, Katoh H. 2005a. Plexins: axon guidance and signal transduction. *Cellular and Molecular Life Sciences* **62**:1363–1371. DOI: <https://doi.org/10.1007/s00018-005-5018-2>, PMID: 15818466
- Negishi M**, Oinuma I, Katoh H. 2005b. R-ras as a key player for signaling pathway of plexins. *Molecular Neurobiology* **32**:217–222. DOI: <https://doi.org/10.1385/MN:32:3:217>, PMID: 16385138
- Neufeld G**, Shraga-Heled N, Lange T, Guttmann-Ravin N, Herzog Y, Kessler O. 2005. Semaphorins in cancer. *Frontiers in Bioscience* **10**:751–760. DOI: <https://doi.org/10.2741/1569>, PMID: 15569615

- Nonaka H**, Takei K, Umikawa M, Oshiro M, Kuninaka K, Bayarjargal M, Asato T, Yamashiro Y, Uechi Y, Endo S, Suzuki T, Kariya KI. 2008. MINK is a Rap2 effector for phosphorylation of the postsynaptic scaffold protein TANC1. *Biochemical and Biophysical Research Communications* **377**:573–578. DOI: <https://doi.org/10.1016/j.bbrc.2008.10.038>, PMID: 18930710
- Nukazuka A**, Fujisawa H, Inada T, Oda Y, Takagi S. 2008. Semaphorin controls epidermal morphogenesis by stimulating mRNA translation via eIF2alpha in *Caenorhabditis elegans*. *Genes & Development* **22**:1025–1036. DOI: <https://doi.org/10.1101/gad.1644008>, PMID: 18413715
- Nukazuka A**, Tamaki S, Matsumoto K, Oda Y, Fujisawa H, Takagi S. 2011. A shift of the TOR adaptor from rictor towards raptor by semaphorin in *C. elegans*. *Nature Communications* **2**:484. DOI: <https://doi.org/10.1038/ncomms1495>, PMID: 21952218
- O'Connor TP**, Cockburn K, Wang W, Tapia L, Currie E, Bamji SX. 2009. Semaphorin 5B mediates synapse elimination in hippocampal neurons. *Neural Development* **4**:18. DOI: <https://doi.org/10.1186/1749-8104-4-18>, PMID: 19463192
- Ohba Y**, Mochizuki N, Matsuo K, Yamashita S, Nakaya M, Hashimoto Y, Hamaguchi M, Kurata T, Nagashima K, Matsuda M. 2000. Rap2 as a slowly responding molecular switch in the Rap1 signaling cascade. *Molecular and Cellular Biology* **20**:6074–6083. DOI: <https://doi.org/10.1128/MCB.20.16.6074-6083.2000>, PMID: 10913189
- Oinuma I**, Ishikawa Y, Katoh H, Negishi M. 2004. The semaphorin 4D receptor Plexin-B1 is a GTPase activating protein for R-Ras. *Science* **305**:862–865. DOI: <https://doi.org/10.1126/science.1097545>, PMID: 15297673
- Ou CY**, Poon VY, Maeder CI, Watanabe S, Lehrman EK, Fu AK, Park M, Fu WY, Jorgensen EM, Ip NY, Shen K. 2010. Two cyclin-dependent kinase pathways are essential for polarized trafficking of presynaptic components. *Cell* **141**:846–904. DOI: <https://doi.org/10.1016/j.cell.2010.04.011>, PMID: 20510931
- Pecho-Vrieseling E**, Sigrist M, Yoshida Y, Jessell TM, Arber S. 2009. Specificity of sensory-motor connections encoded by Sema3e-Plxn1 recognition. *Nature* **459**:842–846. DOI: <https://doi.org/10.1038/nature08000>, PMID: 19421194
- Pellis-van Berkel W**, Verheijen MH, Cuppen E, Asahina M, de Rooij J, Jansen G, Plasterk RH, Bos JL, Zwartkruis FJ. 2005. Requirement of the *Caenorhabditis elegans* RapGEF pxf-1 and rap-1 for epithelial integrity. *Molecular Biology of the Cell* **16**:106–116. DOI: <https://doi.org/10.1091/mbc.e04-06-0492>, PMID: 15525675
- Poinat P**, De Arcangelis A, Sookhareea S, Zhu X, Hedgecock EM, Labouesse M, Georges-Labouesse E. 2002. A conserved interaction between beta1 integrin/PAT-3 and Nck-interacting kinase/MIG-15 that mediates commissural axon navigation in *C. elegans*. *Current Biology* **12**:622–631. DOI: [https://doi.org/10.1016/S0960-9822\(02\)00764-9](https://doi.org/10.1016/S0960-9822(02)00764-9), PMID: 11967148
- Pologruto TA**, Sabatini BL, Svoboda K. 2003. ScanImage: flexible software for operating laser scanning microscopes. *Biomedical Engineering Online* **2**:13. DOI: <https://doi.org/10.1186/1475-925X-2-13>, PMID: 12801419
- Poon VY**, Klassen MP, Shen K. 2008. UNC-6/netrin and its receptor UNC-5 locally exclude presynaptic components from dendrites. *Nature* **455**:669–673. DOI: <https://doi.org/10.1038/nature07291>, PMID: 18776887
- Potkin SG**, Macciardi F, Guffanti G, Fallon JH, Wang Q, Turner JA, Lakatos A, Miles MF, Lander A, Vawter MP, Xie X. 2010. Identifying gene regulatory networks in schizophrenia. *NeuroImage* **53**:839–847. DOI: <https://doi.org/10.1016/j.neuroimage.2010.06.036>, PMID: 20600988
- Rohm B**, Rahim B, Kleiber B, Hovatta I, Püschel AW. 2000. The semaphorin 3A receptor may directly regulate the activity of small GTPases. *FEBS Letters* **486**:68–72. DOI: [https://doi.org/10.1016/S0014-5793\(00\)02240-7](https://doi.org/10.1016/S0014-5793(00)02240-7), PMID: 11108845
- Schmitz C**, Wacker I, Hutter H. 2008. The Fat-like cadherin CDH-4 controls axon fasciculation, cell migration and hypodermis and pharynx development in *Caenorhabditis elegans*. *Developmental Biology* **316**:249–259. DOI: <https://doi.org/10.1016/j.ydbio.2008.01.024>, PMID: 18328472
- Shakir MA**, Gill JS, Lundquist EA. 2006. Interactions of UNC-34 Enabled with Rac GTPases and the NIK kinase MIG-15 in *Caenorhabditis elegans* axon pathfinding and neuronal migration. *Genetics* **172**:893–913. DOI: <https://doi.org/10.1534/genetics.105.046359>, PMID: 16204220
- Shen K**, Bargmann CI. 2003. The immunoglobulin superfamily protein SYG-1 determines the location of specific synapses in *C. elegans*. *Cell* **112**:619–630. DOI: [https://doi.org/10.1016/S0092-8674\(03\)00113-2](https://doi.org/10.1016/S0092-8674(03)00113-2), PMID: 12628183
- Shen K**, Fetter RD, Bargmann CI. 2004. Synaptic specificity is generated by the synaptic guidepost protein SYG-2 and its receptor, SYG-1. *Cell* **116**:869–881. DOI: [https://doi.org/10.1016/S0092-8674\(04\)00251-X](https://doi.org/10.1016/S0092-8674(04)00251-X), PMID: 15035988
- Shitashige M**, Satow R, Jigami T, Aoki K, Honda K, Shibata T, Ono M, Hirohashi S, Yamada T. 2010. Traf2- and Nck-interacting kinase is essential for wnt signaling and colorectal Cancer growth. *Cancer Research* **70**:5024–5033. DOI: <https://doi.org/10.1158/0008-5472.CAN-10-0306>, PMID: 20530691
- Spain SL**, Pedrosa I, Kadeva N, Miller MB, Iacono WG, McGue M, Stergiakouli E, Davey Smith G, Putallaz M, Lubinski D, Meaburn EL, Plomin R, Simpson MA. 2016. A genome-wide analysis of putative functional and exonic variation associated with extremely high intelligence. *Molecular Psychiatry* **21**:1145–1151. DOI: <https://doi.org/10.1038/mp.2015.108>, PMID: 26239293
- Taira K**, Umikawa M, Takei K, Myagmar BE, Shinzato M, Machida N, Uezato H, Nonaka S, Kariya K. 2004. The Traf2- and Nck-interacting kinase as a putative effector of Rap2 to regulate actin cytoskeleton. *Journal of Biological Chemistry* **279**:49488–49496. DOI: <https://doi.org/10.1074/jbc.M406370200>, PMID: 15342639
- Takamatsu H**, Kumanogoh A. 2012. Diverse roles for semaphorin-plexin signaling in the immune system. *Trends in Immunology* **33**:127–135. DOI: <https://doi.org/10.1016/j.it.2012.01.008>, PMID: 22325954

- Tasaka G**, Negishi M, Oinuma I. 2012. Semaphorin 4D/Plexin-B1-mediated M-Ras GAP activity regulates actin-based dendrite remodeling through lamellipodin. *Journal of Neuroscience* **32**:8293–8305. DOI: <https://doi.org/10.1523/JNEUROSCI.0799-12.2012>, PMID: 22699910
- Terauchi A**, Johnson-Venkatesh EM, Toth AB, Javed D, Sutton MA, Umemori H. 2010. Distinct FGFs promote differentiation of excitatory and inhibitory synapses. *Nature* **465**:783–787. DOI: <https://doi.org/10.1038/nature09041>, PMID: 20505669
- Teulière J**, Gally C, Garriga G, Labouesse M, Georges-Labouesse E. 2011. MIG-15 and ERM-1 promote growth cone directional migration in parallel to UNC-116 and WVE-1. *Development* **138**:4475–4485. DOI: <https://doi.org/10.1242/dev.061952>, PMID: 21937599
- Tran TS**, Kolodkin AL, Bharadwaj R. 2007. Semaphorin regulation of cellular morphology. *Annual Review of Cell and Developmental Biology* **23**:263–292. DOI: <https://doi.org/10.1146/annurev.cellbio.22.010605.093554>, PMID: 17539753
- Tran TS**, Rubio ME, Clem RL, Johnson D, Case L, Tessier-Lavigne M, Hugarir RL, Ginty DD, Kolodkin AL. 2009. Secreted semaphorins control spine distribution and morphogenesis in the postnatal CNS. *Nature* **462**:1065–1069. DOI: <https://doi.org/10.1038/nature08628>, PMID: 20010807
- Wang Q**, Charych EI, Pulito VL, Lee JB, Graziane NM, Crozier RA, Revilla-Sanchez R, Kelly MP, Dunlop AJ, Murdoch H, Taylor N, Xie Y, Pausch M, Hayashi-Takagi A, Ishizuka K, Seshadri S, Bates B, Kariya K, Sawa A, Weinberg RJ, et al. 2011. The psychiatric disease risk factors DISC1 and TNIK interact to regulate synapse composition and function. *Molecular Psychiatry* **16**:1006–1023. DOI: <https://doi.org/10.1038/mp.2010.87>, PMID: 20838393
- Wang Y**, He H, Srivastava N, Vikarunnessa S, Chen YB, Jiang J, Cowan CW, Zhang X. 2012. Plexins are GTPase-activating proteins for rap and are activated by induced dimerization. *Science Signaling* **5**:ra6. DOI: <https://doi.org/10.1126/scisignal.2002636>, PMID: 22253263
- Wang Y**, Pascoe HG, Brautigam CA, He H, Zhang X. 2013. Structural basis for activation and non-canonical catalysis of the Rap GTPase activating protein domain of plexin. *eLife* **2**:e01279. DOI: <https://doi.org/10.7554/eLife.01279>, PMID: 24137545
- Weissman JT**, Ma JN, Essex A, Gao Y, Burstein ES. 2004. G-protein-coupled receptor-mediated activation of rap GTPases: characterization of a novel galphai regulated pathway. *Oncogene* **23**:241–249. DOI: <https://doi.org/10.1038/sj.onc.1207014>, PMID: 14712229
- White JG**, Southgate E, Thomson JN, Brenner S. 1986. The structure of the nervous system of the nematode *Caenorhabditis elegans*. *Philosophical Transactions of the Royal Society B: Biological Sciences* **314**:1–340. DOI: <https://doi.org/10.1098/rstb.1986.0056>, PMID: 22462104
- Wu YE**, Huo L, Maeder CI, Feng W, Shen K. 2013. The balance between capture and dissociation of presynaptic proteins controls the spatial distribution of synapses. *Neuron* **78**:994–1011. DOI: <https://doi.org/10.1016/j.neuron.2013.04.035>, PMID: 23727120
- Xuan Z**, Manning L, Nelson J, Richmond JE, Colón-Ramos DA, Shen K, Kurshan PT. 2017. Clarinet (CLA-1), a novel active zone protein required for synaptic vesicle clustering and release. *eLife* **6**:e29276. DOI: <https://doi.org/10.7554/eLife.29276>, PMID: 29160205
- Yamagata M**, Sanes JR, Weiner JA. 2003. Synaptic adhesion molecules. *Current Opinion in Cell Biology* **15**:621–632. DOI: [https://doi.org/10.1016/S0955-0674\(03\)00107-8](https://doi.org/10.1016/S0955-0674(03)00107-8), PMID: 14519398
- Yasuda R**, Harvey CD, Zhong H, Sobczyk A, van Aelst L, Svoboda K. 2006. Supersensitive ras activation in dendrites and spines revealed by two-photon fluorescence lifetime imaging. *Nature Neuroscience* **9**:283–291. DOI: <https://doi.org/10.1038/nn1635>, PMID: 16429133
- Yoo SK**, Pascoe HG, Pereira T, Kondo S, Jacinto A, Zhang X, Hariharan IK. 2016. Plexins function in epithelial repair in both *Drosophila* and zebrafish. *Nature Communications* **7**:12282–12335. DOI: <https://doi.org/10.1038/ncomms12282>, PMID: 27452696
- Zhu JJ**, Qin Y, Zhao M, Van Aelst L, Malinow R. 2002. Ras and Rap control AMPA receptor trafficking during synaptic plasticity. *Cell* **110**:443–455. DOI: [https://doi.org/10.1016/S0092-8674\(02\)00897-8](https://doi.org/10.1016/S0092-8674(02)00897-8), PMID: 12202034
- Zhu Y**, Pak D, Qin Y, McCormack SG, Kim MJ, Baumgart JP, Velamoor V, Auberson YP, Osten P, van Aelst L, Sheng M, Zhu JJ. 2005. Rap2-JNK removes synaptic AMPA receptors during depotentiation. *Neuron* **46**:905–916. DOI: <https://doi.org/10.1016/j.neuron.2005.04.037>, PMID: 15953419